UNIVERSIDADE FEDERAL DO ESPÍRITO SANTO

CENTRO TECNOLÓGICO

DEPARTAMENTO DE ENGENHARIA AMBIENTAL

CLARICE COSWOSK SALLES

CFD SIMULATION OF PARTICLES INJECTION IN THE INLET FLOW OF A SINTER PLANT PRIMARY FABRIC FILTER

VITÓRIA

2020

CLARICE COSWOSK SALLES

CFD SIMULATION OF PARTICLES INJECTION IN THE INLET FLOW OF A SINTER PLANT PRIMARY FABRIC FILTER

Trabalho de Conclusão de Curso apresentado ao Departamento de Engenharia Ambiental e ao Centro Tecnológico da Universidade Federal do Espírito Santo, como requisito parcial para obtenção do grau de Bacharel em Engenharia.

Orientador: Prof. Dr. Rafael Sartim

Co-orientador: Prof. Dr. Bruno Furiei

VITÓRIA

2020

TERMO DE APROVAÇÃO

CFD SIMULATION OF PARTICLES INJECTION IN THE INLET FLOW OF A SINTER PLANT PRIMARY FABRIC FILTER

CLARICE COSWOSK SALLES

Este Trabalho de Conclusão de Curso foi apresentado em 09 de dezembro de 2020 como requisito parcial para a obtenção do título de Bacharel em Engenharia Ambiental e Sanitária. A candidata foi arguida pela Banca Examinadora composta pelos professores abaixo assinados. Após deliberação, a Banca Examinadora considerou o trabalho aprovado.

_____

Prof. Dr. Rafael Sartim
Orientador

_____

Prof. Dr. Bruno Furieri
Co-orientador

_____

Profª. Dra. Elisa Valentim
Convidada Interna

_____

Ma. Ana Clara Bernabé
Convidada Interna

AGRADECIMENTOS

Certamente estes parágrafos não irão atender a todas as pessoas que fizeram parte dessa importante fase da minha vida. Portanto, desde já peço desculpas àquelas que não estão presentes entre essas palavras, mas elas podem estar certas que fazem parte do meu pensamento e de minha gratidão.

Agradeço ao privilégio de ter sido aluna do corpo docente do Curso de Engenharia Ambiental pela Universidade Federal do Espírito Santo. Ao meu orientador Rafael Sartim, pela confiança que depositou em mim desde que nos conhecemos, se tornando um espelho que tenho na vida. E ao meu co-orientador Bruno Furieri, por me guiar nessa trajetória com sua sabedoria e exemplo.

Aos meus colegas de sala, obrigada pela parceria e por tornarem esses 5 anos mais leves. Sempre ajudando um ao outro, na vida e na faculdade, e comemorando cada conquista. Em especial agradeço a Marina que me aguentou 24 horas por dia em sala da aula, estágio e saideiras do final de semana. Também tenho gratidão aos meus amigos veteranos e de outras engenharias, guardo um carinho especial por vocês que se tornaram grandes amigos.

À Ana Clara e Elisa, por aceitarem o convite para participar dessa banca examinadora. Vocês são referências para mim nessa área que escolhi atuar.

Gostaria de deixar registrado também, o meu reconhecimento aos meus pais, José Leandro e Regina, pois acredito que sem o apoio deles seria muito difícil vencer esse desafio. À minha irmã, Júlia, e meu cunhado Guilherme, pelo amor e carinho que me ajudaram e seguir em frente nessa caminhada.

Aos meus amigos de adolescência e infância, Bruna, Ana Carolina, Mariana, Carol Martins, Beatriz, Isabela, Bárbara e Lara por sempre acreditarem em mim e vibrarem comigo em cada conquista. Essa também é de vocês.

E meu último, mas não menos importante, agradecimento vai ao meu namorado Igor que esteve ao meu lado todos os dias durante a construção desse trabalho. Sua ajuda e apoio nessa fase foi essencial para que eu chegasse até aqui.

ABSTRACT

The knowledge of the negative impacts of air pollution culminated in the need to control sources of pollution and establish emission limits. Ducted particulate matter emissions through stacks can represent a large part of the steel industry emission, so, to comply with legislation standards, the industry uses air pollution control equipment. A widely used device is the fabric filter, which retains the particles in the gas flow through a series of fabric bags. A premise for good filtration efficiency is that the gas flow is evenly distributed, in such a way that all the bags are subject to the same velocity and pressure. Thus, designers seek to make improvements in the geometry of the equipment entrance duct to meet this premise. Another practice widely used to improve filtration performance is the precoating technique, in which hydrated lime is injected into the filter inlet duct to cover the fabric bags, preventing them from corrosion and clogging of the pores. This material distribution at the equipment entrance must be as uniform as the gas flow, to cover all the bags equally with hydrated lime. With the evolution of computational resources and software, analysis of this equipment design can be performed using the computational fluid dynamics (CFD) technique, both in retrofit cases and in the design of new filters. Therefore, this work aims to investigate the characteristics of gas flow and hydrated lime injections in the inlet duct of an existing industrial fabric filter. For this, the simulations were performed with the CFD tool, using the Euler-Lagrange approach to simulate the gas-solid two-phase flow. After this analysis, it was possible to evaluate how the geometry of the inlet duct influences the distribution of the gas-solid flow, consequently, the efficiency of the filtration process. Then, the analysis of two scenarios was carried out: the first was of the existing geometry of the duct work and the second was with a change in the design, in which the bypass of the main duct was removed. In the existing duct scenario, it was observed that the bypass generates a strong influence on the gas flow pattern, which in turn directly affects the hydrated lime distribution, causing low-velocity recirculation areas that are subject to particle deposition. In the second scenario there was a more homogeneous gas flow distribution and a reduction of 52,60% of the total pressure drop in the system. However, it was observed that, among the eight duct outlets on each side, the second ones contained lower air velocity, less gas streamlines, and hydrated lime mass flow close to zero. This highlighted result was not caused by the presence of the bypass, but by the configuration of the duct outlets. Therefore, the filtration bags are subject to different amounts of hydrated lime, gas velocity and pressure, reinforcing the need for design improvements at the equipment entrance geometry.

RESUMO

O conhecimento dos impactos negativos da poluição do ar culminou na necessidade de controlar fontes de poluição e estabelecer limites de emissão. Emissões pontuais de material particulado através de chaminés podem representar grande parte das emissões de uma siderurgia, logo, para cumprir os padrões da legislação, a indústria utiliza equipamentos de controle da poluição do ar. Um equipamento amplamente utilizado é filtro de mangas, que retém as partículas existentes no fluxo de gás através de uma série de mangas de tecido. Uma premissa para uma boa eficiência da filtração é que o fluxo de gás esteja uniformemente distribuído, de tal forma que todas as mangas estejam sujeitas à mesma velocidade e pressão. Assim, os projetistas buscam realizar melhorias na geometria do duto de entrada desse equipamento para atender a essa premissa. Outra prática muito utilizada para melhorar a performance de filtração é técnica do *precoating,* na qual injeta-se cal hidratada no duto de entrada do filtro para cobrir as mangas de tecido, prevenindo-as da corrosão e o entupimento dos poros. A distribuição desse material na entrada do equipamento deve ser tão uniforme quanto o fluxo de gás, para que todas as mangas sejam cobertas igualmente com a cal hidratada. Com a evolução dos recursos computacionais e dos softwares, análises do design destes equipamentos podem ser realizadas por meio da técnica de fluidodinâmica computacional (CFD), tanto em casos de retrofit, quanto no projeto de novos filtros. Logo, esse trabalho objetiva investigar as características do escoamento de gás e das injeções de cal hidratada no duto de entrada de um filtro de mangas industrial existente. Para isso, as simulações foram realizadas com a ferramenta de CFD, utilizando a abordagem Euler-Lagrange para simular o escoamento bifásico gás-solido. Após essa análise, foi possível avaliar como a geometria do duto de entrada influencia na distribuição do escoamento gás-sólido, consequentemente, na eficiência do processo de filtração. Realizou-se, então, a análise de dois cenários: o primeiro foi da geometria existente do conjunto de dutos e o segundo foi com uma alteração no design, na qual removeu-se o by-pass do duto principal. No cenário do duto existente foi possível observar que o by-pass gera forte influência no padrão de escoamento de gás que, por sua vez, afeta diretamente na distribuição de cal hidratada, provocando zonas de recirculação com baixa velocidade que são sujeitas à deposição de partículas do material alcalino. No segundo cenário apresentou-se uma distribuição do fluxo de gás mais homogêneo e uma redução de 52,60% da perda de carga total no sistema. Entretanto, foi observado que, dentre as oito saídas do duto existentes em cada lado, as segundas continham menor velocidade do ar, menos linhas de corrente e fluxo mássico de cal hidratada perto de zero. Esse resultado, em destaque, não foi ocasionado pela presença do by-pass, mas sim pela configuração das saídas do duto. Logo, as mangas de filtração estão sujeitas a diferentes quantitativos de cal hidratada, velocidade e pressão do gás, reforçando a necessidade de melhorias no design da entrada do equipamento.

Palavras-chave: Filtro de mangas. Dinâmica dos Fluidos Computacional. Escoamento bifásico. Poluição atmosférica. Material Particulado.

ILLUSTRATION LIST

TABLE LIST

TABLE OF CONTENTS

1 INTRODUCTION

In 1989, the National Environment Council (CONAMA), in compliance with Resolution No. 5 and guided by the powers conferred on it by Law No. 6.939, instituted the National Air Quality Control Program (PRONAR). This resolution aims to impose limits on national emissions according to the sources and priority pollutants. It was necessary to establish strategies for the control, preservation, and recovery of air quality (BRASIL, 1989). With this historic advance, in 2006, CONAMA Resolution No. 382 was created, which established the maximum limits for the emission of air pollutants to fixed sources installed or with a license application before second January 2007 (BRASIL, 2006), updated in 2011 to CONAMA Resolution No. 436.

There are many air pollutants, with different dangers to human health, public welfare, or materials, fauna, and flora. PM (Particulate Matter) associates with chronic effects on the respiratory and cardiovascular system in the exposed population. Approximately 3% of cardiopulmonary and 5% of lung cancer deaths are attributable to PM globally (WHO, 2013). According to the WHO Global Ambient Air Quality Database updated in 2018 (WHO, 2020), it was estimated that around 7 million people die every year from exposure to fine particles in polluted air. Besides, using data from the Informatics Department of the Brazilian Unified Health System (DATASUS), probable premature deaths were identified due to long-term exposure to $PM_{2,5}$, namely: 9,700 premature deaths in the capital of São Paulo and 3,900 premature deaths in the cities of Rio de Janeiro, Belo Horizonte, Porto Alegre and Curitiba (ANDREÃO; ALBUQUERQUE; KUMAR, 2018). It should also be noted that these premature deaths could be prevented if the pollutants' concentrations were in compliance with WHO guidelines. Even that policy-makers set air quality standards in many countries to protect public health, such a reality is present in most of the developing countries, given that PM concentrations exceeded the latest air quality guidelines set by the WHO for mean annual exposures to PM_{10}[1] (20 $\mu g\ m^{-3}$) (KIM; KABIR; KABIR, 2015).

Outdoor PM pollution mainly comes from motor vehicles, wood-burning heaters, and industry (WHO, 2013). Among these activities, the steel industry is a notable source of PM emissions. According to Hasanbeigo, Khanna, and Price (2017), this industry is the second-largest PM emitter, behind only the cement company. The

[1] Particulate matter with na aerodinamic diameter less than 10 µm.

emissions occur by stationary sources (chimneys) in all stages of the steelmaking process: coking, sintering, pelletizing, blast furnace, melt shop, rolling mill, and cast-house (DAI et al., 2015). In addition to the mentioned activities, mobile sources (circulation of vehicles on the access roads) and diffuse sources (wind erosion of raw material storage piles) also emit PM (LI et al., 2009).

Given the importance of controlling sources of PM pollution and limiting the impacts of air quality on human health, the steel industry's quest to improve itself to meet the environmental standards became evident. Dedusting systems are needed to reduce the PM emission rates and reach the limits stablished by the local regulation. Therefore, the dedusting process takes place by a local exhaust ventilation system, in which the pollutants emitted by a source are captured through hoods located in the emission origin. Then, the depression produced by the fan conducts the air with the pollutants through a ductwork to the control equipment. Finally, the pollutants are treated by devices that retain particles or dissolve gases, and, subsequently, the clean air is released into the atmosphere through the stack (ACGIH, 2019a).

Among the technologies available, the major dust collector devices used are fabric filters, electrostatic precipitators, cyclone towers, and wet scrubbers. The fabric filter is the most applied in the industries due to its efficiency and cost-benefit (ROCHA et al., 2014). Its working principle bases on the filtration of the gas containing PM in an upward flow through a series of fabric bags (porous medium). Subsequently, the particles retained by the fabric discharge into the bottom of the equipment, and clear air flows through the top (COOPER; ALLEY, 2011). At the filter medium, PM filtration is divided into two steps. In the first one, when the bag is virgin, the particles are collected through the mechanisms of inertial impaction, interception, and diffusion. In the second, known as surface filtration, the particles trapped in the fibers along the filtration period build up a superficial layer of PM (filter cake) that becomes the primary filtration medium (DULLIEN, 1989). There comes a time when the filter cake settles in the fabric, decreasing the operation efficiency, and requiring the cleaning of the filter medium to maintain the system pressure drop at a stable level. The most common cleaning mechanisms are: shaking, reverse air, pulsating, and sonic jet (USEPA, 2002). However, according to Schnelle and Brown (2002), the most usual method is through pulsating air jets that use concise blasts of compressed air to deform the bag and remove the trapped material.

For Pereira et al. (2016) the filter efficiency depends on the choice of the filter medium (the fabric of the bags), the equipment design and the process variables such as inlet pressure and velocity, and chemical and physical characteristics of the gas (pH, viscosity, temperature, among others). Besides, the number of the cleaning cycles of the filter medium is related to its lifetime, which is an essential economic variable since the material has a high replacement cost. In this context, the ideal would be that for each application, a specific filter would be designed instead of a generic one, which is what occurs today.

To obtain greater operation efficiency, and longer service life of the bags, currently designers seek to design geometries so that the gas inlet flow is as uniform as possible (ROCHA et al., 2014). This condition is essential because a filter with a non-homogeneous gas flow distribution provides areas with a higher or lower filtration velocity than that specified by the project. For instance, in regions with very high filtration velocity, it can cause the wear of the bags, which reduces their service life span; and areas with very low filtration velocity will decrease operation efficiency (DAMINAN et al., 2004).

Improvement of the filter medium is another common practice to increase particle collection efficiency. Among the usual methods, there are selection of the fabric material, treatment of the bags fabric, and precoating. However, precoating is considered a promising alternative given its excellent results in increasing particle collection efficiency, simplicity, and lower cost (ANDRADE; SARTIM; AGUIAR, 2019). The method consists of covering the new filter medium (nonwoven fabric) with particulate material, preventing the clogging of the bag by the penetration of sub micrometric particles. The content assists in the dust cake initial formation, ensuring surface filtration, and preventing early saturation of the filter medium (ANDRADE, 2019). Furthermore, filters with precoating favor a better cake detachment from the surface, facilitating its cleaning (RAVERT, 2006). Schiller, Hellmich, and Schmid (2016) highlight that the use of hydrated lime powder for precoating reasons demonstrates proper functioning at affordable costs, plus Andrade, Sartim, and Aguiar (2019) point that this material is widely used in the steel industry's precoating of fabric filters. In addition to the choice of material powder, a premise for excellent precoating efficiency is that the powder distribution in the filter compartment and bags is uniform, as a result of homogeneous gas flow and velocity (SCHMIDT; LÖFFLER, 1990).

Considering the importance of homogeneous fluid flow and precoating powder distribution in a fabric filter with a uniform filtration velocity, the improvement of such a design parameter configures a mechanics engineering problem, which can be analyzed by analytical, numerical methods, and laboratory experimentation. However, analytical methods are limited to solve complex problems, and laboratory experimentation takes a long time and has high costs. In this scenario, numerical simulation has stood out to solve complex problems with complex geometries and general boundary conditions, presenting results more quickly (MALISKA, 2004). With the growth of computational resources and the development of different simulation software, this method has become increasingly flexible, which has also contributed to reduce its cost (ROCHA et al., 2014).

The CFD (Computational Fluid Dynamics), is a numerical method that promotes a thorough evaluation of the dynamics flow in processes and inside equipment, making it possible to optimize its operation (VERSTEEG; MALALASEKERA, 2007). It is a powerful tool because it is capable of using real data in its simulations, getting closer and closer to reality.

In this context, previous works such as those by Nielsen et al. (2011), Rocha et al. (2014), Pereira et al. (2016), Bernabé (2016), Oliveira (2018), Lima (2019) and Park et al. (2019), presented the broad application of the CFD in optimizing the performance of fabric filters by modifying its design, after understanding the flow dynamics inside it. Additionally, other authors such as Adam et al. (1996), Zhang and Li (2008), De Almeida Santos et al. (2012), Shi et al. (2017), and Chang et al. (2019) showed the possibility of simulating two-phase flows dynamics to optimize the gas-solid distribution in ventilation system ducts and, thus, increase the dedusting efficiency. This tool has also appeal to decision making for new projects besides retrofit ones (BERNABÉ, 2016).

Given the enormous potential that CFD presents to solve engineering problems with gas-solid two-phase flows, the present work intends to explore this tool in a real engineering case. Therefore, a two-phase numerical simulation with the commercial software Fluent was carried to investigate fluid and hydrated lime particles behavior based on an existing Sinter Primary Fabric Filter inlet duct, aiming to analyze its influence in the fabric filter inlet flow and performance.

2 OBJECTIVES

2.1 GENERAL OBJECTIVE

This work aims to understand how the geometry of the fabric filter inlet duct system influences the gas-solid inlet flow in the filter compartments, comparing the existing duct scenario with another scenario with design modifications, and using computational fluid dynamics.

2.2 ESPECIFIC OBJECTIVES

- Evaluate the fluid flow distribution at the existing duct;
- Evaluate the distribution of hydrated lime injections inside the existing duct;
- Compare the gas and particle flow results with another scenario with geometries modifications in the duct;
- Evaluate the influence of the existing duct geometry in the gas-solid two-phase flow distribution in the fabric filter compartment.

3 LITERATURE OVERVIEW

3.1 AIR POLLUTION

According to Brazilian legislation's CONAMA Resolution No. 491 of 19/11/2018, which revoked and replaced CONAMA Resolution No. 3 of 28/06/1990, an air pollutant consists of:

> "(…) any form of matter in quantity, concentration, time or other characteristics, which make or may render the air inappropriate or harmful to health, inconvenience public well-being, harmful to materials, fauna, and flora or harmful safety, the use and enjoyment of the property or the normal activities of the community."

For the World Health Organization (2019), the most common air pollutants are Particulate Matter (PM_{10} and $PM_{2,5}$), Ozone (O_3), Nitrogen Dioxide (NO_2), Carbon Monoxide (CO), Sulfur Dioxide (SO_2) and Volatile Organic Compounds (VOC's).

3.1.1 Particulate Matter

PMs are small solid particles and liquid droplets suspended in the air formed by various compounds such as inorganic ions, organic compounds, and metals. Anthropogenic sources of PM include combustion engines (both diesel and petrol), solid-fuel (coal, lignite, heavy oil and biomass) combustion for energy production in households and industry, as well as other industrial activities (building, mining, manufacture of cement, ceramic and bricks, and smelting). Natural PM sources include volcanoes, dust storms, forest fires, living vegetation, and sea spray. Nevertheless, particle pollution mainly comes from motor vehicles, wood-burning heaters, and industry (WHO, 2013).

The health-hazardous associated with PMs are distinct by their size (WHO, 2013):

- PM_{10} (particles with a diameter of 10 micrometers or less): also considered as inhalable particles; they are small enough to pass

through the throat and nose and enter the lungs. When inhaled, these particles can affect the heart and lungs, causing severe health effects;

- $PM_{2.5}$ (particles with a diameter of 2,5 micrometers or less): also known as breathable particles ou fine particles, they are so small that they can get deep into the lungs and into the bloodstream. Evidence point that exposure to $PM_{2,5}$ over periods of years can cause adverse health damages.

While the nasal cilia and the mucus can filter most of the particles bigger than 10 µm, smaller particles can penetrate deeper the respiratory tracts, tracheobronchial tree, respiratory bronchioles, and lung alveoli. The second one has the most impact on human health effects since those between 1 and 5 µm can penetrate the circulatory system, causing severe damage. Among the effects of PM exposure on human health, Kim, Kabir, and Kabir (2015) list premature deaths, increase in hospital admissions and emergency room visits, respiratory infections including asthma and pneumonia, chronic bronchitis, cancer, cardiovascular diseases, diabetes, and chronic obstructive pulmonary diseases.

According to the World Health Organization (2013), various studies show relations between exposure to particles and increased hospital admissions such as death from heart or lung diseases. Approximately 3% of cardiopulmonary and 5% of lung cancer deaths are attributable to PM globally. In the WHO Global Ambient Air Quality Database updated in 2018, it was estimated that around 7 million people die every year from exposure to fine particles in polluted air.

Andreão, Albuquerque, and Kumar (2018) investigated the correlation between the concentration of $PM_{2,5}$ and the health effects of the population of 24 Brazilian cities, among which 89% of the total annual data analyzed were above the WHO guidelines (10 µg m^{-3}). Using data from the Informatics Department of the Brazilian Unified Health System (DATASUS), probable premature deaths were identified due to long-term exposure to $PM_{2,5}$, namely: 9.700 premature deaths in the capital of São Paulo and 3.900 premature deaths in the cities of Rio de Janeiro, Belo Horizonte, Porto Alegre, and Curitiba. The authors also noted that these premature deaths could be prevented if the pollutants' concentrations were in compliance with the standards. Such a reality is present in most developing countries, given that PM

concentrations exceeded the latest air quality guidelines set by the WHO for mean annual exposures to PM_{10} (20 μg m^{-3}) in most of the cases (KIM; KABIR; KABIR, 2015).

Given the irregularities on PM emission levels and their effects on public health, policymakers set air quality standards in many countries to protect public health. Moreover, numerous legislation in Brazil and around the world established PM emission standards for fixed sources to decrease human and environmental hazards.

3.1.2 PM Emission Standard

According to Brasil (2006), emission standards are the maximum level of pollutants emitted by a source allowed. It is an environmental control tool associated with the criteria of ecological support capacity. The resolution CONAMA 382/2006 establish emission limits of air pollutants for fixed sources, as well for each fuel source utilized, with the installation before its validity (January 2007). In 2011 resolution CONAMA 436/2011, created to complement CONAMA 382/2006, established air pollutants emission limits for fixed sources with installation after and before 2007.

Table 1 disposes the federal PM emission standards in CONAMA 436/2011 resolution for the steel production processes: Coke Oven, Sintering, Coke Blast Furnace, Blast Furnace, LD Melt Shop, Electric Melt Shop, Hot Strip Mill, Pelletizing and Power Plant.

Table 1: Maximum PM emission limits for steel industry according to CONAMA 436/2011.

Production Unity	Fixed emission source	PM emission limit (mg/Nm³)
Coke Oven	Cokeside Dedusting System	40
	Coke Furnace Combustion Chamber	50
Sintering	Primary Dedusting System	70
	Secondary Dedusting System	70
Coke Blast Furnace	Dedusting System of the Stock House	40
	Dedusting System of the House or Race Wing	40
Blast Furnace	Dedusting System of the Storage House	50
	Dedusting System of the House or Race Wing	50
LD Melt Shop	Primary Dedusting System	80
	Secondary Dedusting System	40
	Pig Iron Desulfurization Dedusting System	40
	Lime Furnace Dedusting System	100
Hot Strip Mill	Reheat Furnaces with Burning Steel Gases	60
Pelletizing	Exhaust System of Pelletizing Furnance	70

Source: Adapted from CONAMA 436/2011.

In this context, to meet the emission limits of federal and local standards and improve de environmental performance of industries, it is necessary to adopt technologies to control atmospheric pollutants emission that are technically and economically viable and accessible and already developed on a scale that allows their practical application. Moreover, these increasingly restrictive legal limits show the need to anticipate the future in the search for technological alternatives to enhance the efficiency of such air pollution control technologies.

3.2 LOCAL EXHAUST VENTILATION SYSTEM

Local exhaust ventilation systems are recommended as the best practice for air pollution control techniques (ACGIH, 2019a). It has the main objective of capturing and treating pollutants from sources (gases, vapors, or toxic dust) before they disperse in the work environment and the surrounding community's atmosphere. The system's components are hoods, ductwork, air cleaning device, fan, and stack (Figure 1). In this way, the pollutants emitted by a source are captured through the hoods located in the emission origin. Then, the depression produced by the fan conducts the air with the pollutants through ductwork to the control equipment. Finally, the pollutants are treated (by devices that retain particles or dissolve gases), and, subsequently, the clean air is released into the atmosphere through the stack. ACGIH (2019a) has the best practice recommendations for most industrial processes and operations, as a guideline to be followed. Also, the system's maintenance and operation procedures are set out in the ACGIH (2019b).

Figure 1: Scheme of a local exhaust ventilation system.

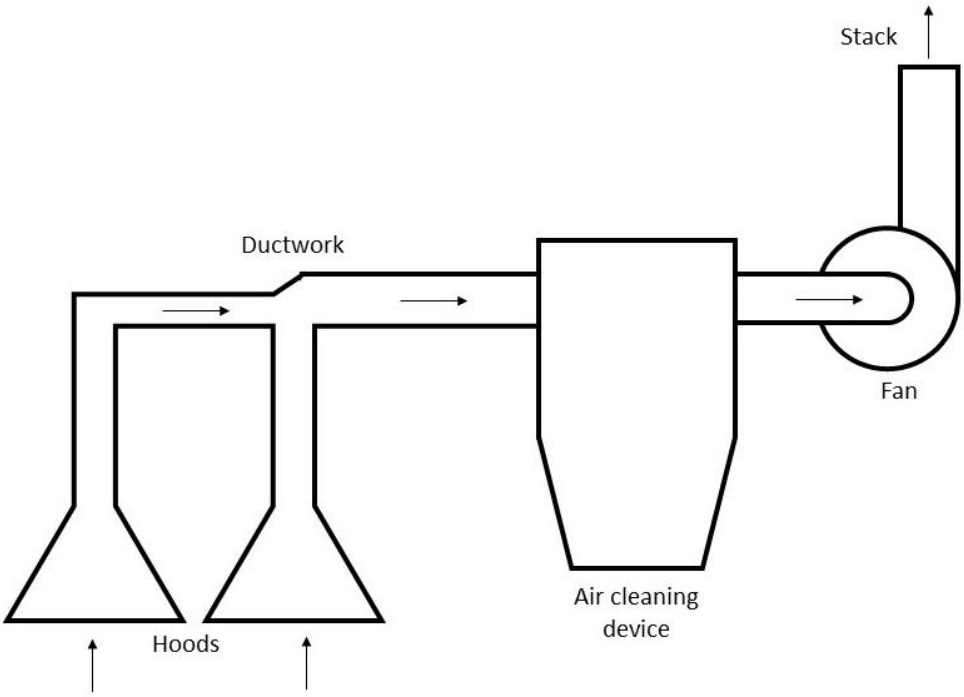

Source: Own authorship.

As this work focusses on local exhaust ventilation system applied on particulate matter emission control, in the steel industry, this combination is typically called a dedusting system. Therefore, most usual dust collector devices in dedusting systems are cyclones, fabric filters, electrostatic precipitators, and wet scrubbers. In all of this equipment, solid-gas separation occurs by applying one or more forces. These include gravitational, inertial, centrifugal and electrostatic forces, causing the particle to accelerate in its direction but away from the flow. These particles are then removed from the system to prevent them from returning to the flow (COOPER; ALLEY, 2002).

The cyclone is a mechanical collector with a great advantage of low installation and maintenance costs; on the other hand, it has the disadvantage of presenting low efficiency (especially for small particles), resulting in high energy expenditure due to pressure drop. Electrostatic precipitators are very efficient equipment (even for smaller particles) and generate low pressure-drop; however, the operational cost is high due to energy expenditure. Although wet scrubbers are efficient for fine particles/droplets collection, the increase of efficiency demands high operating costs and water volume, which, in turn, raises costs with wastewater treatment. In this scenario, Cooper and Alley (2002) explain that each air pollution control problem is unique and requires an engineering solution. However, the fabric filter stands out in the industries due to its simplicity, efficiency, and cost-effectiveness (ROCHA et al., 2014). Such a device can operate with a wide range and filtrate acid gases. Moreover, it can be compartmentalized to avoid interruptions in operation when maintenance is required. In general, even with these advantages, fabric filters have high pressure-drop and maintenance cost and do not operate with high-temperature applications in the fluid.

3.3 FABRIC FILTER

The operation of the fabric filter consists of the filtration of a gas that contains particles through fibers of fabric called bags. In the process, the gas, exhausted by a local exhaust ventilation system, enters the equipment typically from the bottom (hopper) and flows in an upward flow through the bags (porous medium), where the filtration of the particles occurs (SCHNELLE; BROWN, 2002). Then, the filtered particles discharge into the hopper, the lower region of the equipment, and the clean air rises in the upper zone. The particle capture is divided into two steps. In the first one, when the operation is started, the particles are collected through the mechanisms of inertial impaction, interception, and diffusion. This step is also called as depth filtration. In the second one, known as surface filtration, the particles trapped in the fibers along the filtration period build up a superficial layer of particulate matter (filter cake) that becomes the primary filtration medium (DULLIEN, 1989). There comes a time when the filter cake accumulates in the fabric, decreasing the operation efficiency, and requiring the cleaning of the filter medium to maintain the system pressure drop at a stable level. Among the bags cleaning mechanisms, the most common are: mechanical shaking, reverse air, and pulsating jet (USEPA, 2002). However, according to Schnelle and Brown (2002), the most usual method is pulsating air jets that use concise blasts of compressed air to expand the bag and remove the trapped material.

Figure 2 presents the schematic of ta fabric filter components with a pulse-jet cleaning system. According to USEPA (2002), the main components of a fabric filter are: the bags supported vertically by a cage at the top of the equipment; the equipment carcass or chamber; the hopper in the lower region; the discharge mechanism to unload the particulate material deposited in the hopper, which can be manual or automatic; the tube sheet where the cages and bags are fixed; and the cleaning system which is represented by the pulse-jet mechanism. Additionally, the baffle indicated in the image is a common component in fabric filters to improve the inlet flow distribution between the bags.

Figure 2: Schematic of fabric filter operation with pulse-jet cleaning system.

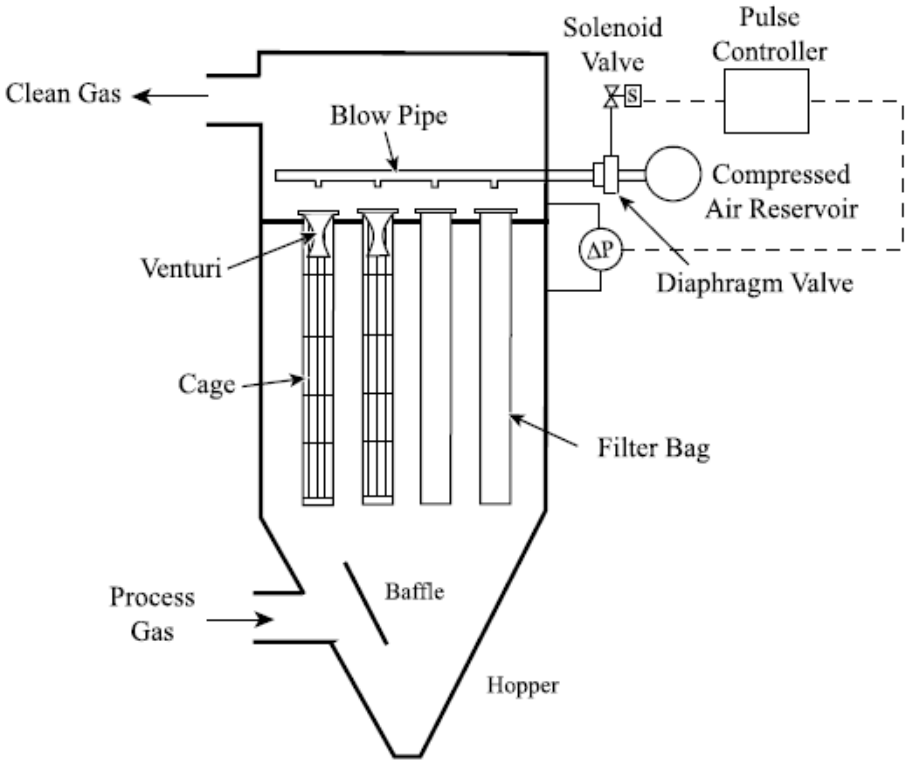

Source: Schnelle and Brown (2002).

For Wang, Pereira, and Hung (2004), fabric filter efficiency is related to operational parameters, such as system pressure drop, the fabric of the bags (filter medium), cleaning mechanism, air-to-cloth ratio, and the equipment geometry. Thus, the ideal would be that for each application, a specific filter would be designed instead of a generic one, which is what occurs today. For instance, it is generally assumed that, to simplify the calculations, the flow at the filter inlet is uniform and that all the bags are subjected to the same values of air-to-cloth ratio and pressure. However, previous using CFD simulation identified an non uniform pattern on the bags (BERNABÉ, 2016; PEREIRA, 2016) which is not seen in practice (verbal information)[2]. Therefore, some designers seek to modify the duct inlet geometry to obtain a better flow distribution and a homogeneous air-to-cloth ratio in the bags.

The air-to-cloth ratio, also called as the filtration velocity, is the gas flow rate divided by the fabric collection area (SCHNELLE; BROWN, 2002). The numerical value is given by Equation 1.

$$Air - to - Cloth\ Ratio = \frac{Total\ Flow}{Filtration\ Area} \quad (1)$$

[2] Rafael Sartim gave information in may 2020.

The air-to-cloth ratio is given in a unit of velocity, usually m min^{-1}. It can be interpreted as the velocity that passes through the bag in the normal direction to its surface, given the flow definition itself. This parameter is essential for a fabric filter efficiency since a lower air-to-cloth ratio provides a more extensive collection area, so dust cake buildup and pressure drop increase at a lower rate than a high air-to-cloth ratio (SCHNELLE; BROWN, 2002). Besides, high filtration velocity values provide a small filtration period, and thus, particle penetration in the bag increases, which, in turn, makes dust cake removal difficult, increasing residual pressure drop and bags clean frequency, and reducing its service life span (ROCHA, 2010).

Another significant parameter for a better flow distribution is the filter house geometry and its inlet duct design. The inlet design configuration can have a direct bearing on bag service life because a filter with a non-homogeneous gas flow distribution provides areas with a filtration velocity higher or lower than that specified by the project. In regions with very high velocity, it can cause the wear of the bags, reducing their service life span; at the same time, areas with very low velocities may indicate low filtration efficiency (DAMINAN et al., 2004). This condition can also cause dust re-entrainment from the hopper, since the inlet is typically near, or directed toward the bottom of the bags, dust entrained in the high-velocity streamlines can abrade the bags, especially at the bottom (ALLEY; COOPER, 2002).

Considering the importance of homogeneous fluid flow distribution in a fabric filter with a uniform filtration velocity, the improvement of such a design parameter configures a mechanics engineering problem, which has been analyzed by fabricants know how and empirical methods. However, analytical methods are unable to solve complex problems, and laboratory experimentation takes a long time and has high costs. In this scenario, numerical simulation has stood out for being able to solve complex problems with complex geometries and general boundary conditions, presenting results more quickly (MALISKA, 2004). Furthermore, with the growth of computational resources and the development of different simulation software, this method has become increasingly flexible, which has also contributed to the reduction of its cost (ROCHA et al., 2014).

The CFD (Computational Fluid Dynamics) is a numerical method that promotes a thorough evaluation of the dynamics flow in processes and inside equipment, making it possible to optimize the filter's design and efficiency

(VERSTEEG; MALALASEKERA, 2007). It is a powerful tool because it is capable of using real data in its simulations, getting closer and closer to reality. Also, this technique has appeal to decision making during the conception of new projects (BERNABÉ, 2016).

In this context, previous works, such as those by Damian et al., (2004), Nielsen et al. (2011), Rocha et al. (2014), Pereira et al. (2016), Bernabé (2016), Oliveira (2018), Lima (2019), and Park et al. (2019), presented the broad application of the CFD tool in optimizing the performance of fabric filters and dedusting system by proposing some geometry improvements, after understanding the flow dynamics inside it.

3.3.1 Correlated Works

In your work, Damian et al. (2004) utilized the CFD to evaluate exhaust gases' behavior and improve the performance of an asphalt industry dedusting system. The authors carried out a CFD analysis of the fluid flow inside a previous fabric filter in the fabric, using the CFX-5 software. In this equipment, it was observed that some filtering bags had a short service life. The simulation showed that the air had a very non-uniform distribution, originated by the rough air inlet shape. So, to improve the inlet flow distribution, a new gas inlet was proposed with the application of deflectors. Field measurements result verified that this inlet geometry improvement promoted a pressure drop decrease from 800 Pa to 350 Pa, considering the same filtering area. Additionally, this result increased the fabric filter efficiency, making it possible to reduce its dimensions and, consequently, reduce the exhaust fan energy consumption, leading to a more economical asphalt plant. This work was a great precursor for CFD simulation in fabric filter, initiating a series of computational fluid dynamics analyzes in such control equipment. Furthermore, the authors proposed the use of polyester pleated bags, avoiding the bag failure due to high temperature or low-temperature operation, besides the use of a pre-separator before the fabric filter, allowing a better dust collection efficiency.

Nielsen, Skriver, and Castaño (2011) carried out three case studies to retrofit existing fabric filters and an electrostatic precipitator (EP) using CFD, demonstrating the tool's potential in the design, testing, and comparison of different solutions. For the simulations, the authors used the commercial CFD code STAR-CD. The first case was

adapted from existing equipment and, due to the size limitation, premature failures in the filter bags were observed. After analyzing the simulation results, it was suggested the installation of deflectors into the flow inlet hopper. With this improvement, the velocity distribution was highly optimized, generating an increase in the bags' service life by 400%. The second case studied showed worn filter bags due to the abrasion of the filter material. Thus, design modifications included the application of deflectors in part of the inlet duct and in the compartments, which also demonstrated a better gas velocity distribution. The third case, on the other hand, reported problems of unbalanced flow, premature wear of filter bags, and dust settling in regions of the filter. Applying deflectors at the entrance and on the hopper wall, there were improvements concerning the maximum velocities found in the filter bags' vicinity and the velocity distribution in the equipment. This change could lead to an increase in the bags useful life; however, the modification was not implemented but helped to achieve small adjustments. Finally, the electrostatic precipitator case required significant maintenance efforts to comply with new regulations (more restrictive emission standards). Thus, EP conversion to a fabric filter was studied with the installation of inlet ducts with dampers and baffles in each compartment, which caused a better distribution of velocities. In general, the authors presented the tool's vast usefulness in optimizing air pollution control equipment and the savings and efficiency that simulations bring when evaluating various possibilities.

Rocha et al. (2014) used CFD to simulate the dynamics of a single-phase flow in an industrial fabric filter to investigate the best position for the gas to enter the equipment. Two different inlet positions were simulated: conventional feeding, in which the gas comes into contact with the bags through the center in a single inlet and triple feeding, in which three inlets receive the same gas flow, at the top, center, and bottom of the filter medium. The simulations were performed using the ANSYS Fluent v13.0 software. In the results, the design with conventional entry showed high-velocity regions, which can be associated with the premature wear of the bags observed compared to other parts of the filter. The triple inlet geometry, on the other hand, provided greater efficiency in performance, due to its better distribution of the flow in the filtering medium and less pressure drop, increasing the service life span of the bags.

In another study, Pereira et al. (2016) used the same geometry and conditions as Rocha et al. (2014) but to analyze how the position of the inlet flow of the filter

influences the internal air profile and the filtration performance. For the simulation, ANSYS Fluent v13.0 software used. They tested four different inlet configurations:

1) A simple entry in the bottom region of the filter with the upward flow;
2) Conventional entrance in the center, directly impacting the bags and spreading over the rest of the equipment;
3) Double and opposite entrance in the lower region, similar to the single entrance;
4) Tangential inlet on the side, with airflow around the filter and through the bags.

The simulations showed that the inverted double inlet configuration was more appropriate. The mass flow inside the equipment in this condition was more uniform, making the filter more efficient and the bags lasting.

Bernabé (2016) also proposed retrofit of an existing fabric filter in the steel industry using CFD to study the characteristics of the gas flow inside it and to analyze distinct inlet geometry proposals for improving the distribution of the gas flow in the bags. The author used the ANSYS CFX v16.0 software. In addition to the reference case, three more alternatives were simulated:

1) A 60% reduction in the project flow;
2) Division of the single duct inlet into two with the same stream;
3) Installation of deflectors in the inlet duct;

Since the first alternative presented the best results in terms of increasing the percentage of the filtration area (79,9% of the reference case to 85,1%), the author proposed two other alternatives: 4) flow reduction and division the inlet duct in two and; 5) flow reduction and installation of deflectors. The best option was the second one because it promoted a proper filtering velocity distribution through the bags. In this simulation, vortices in the hopper's bottom observed in the reference case were reduced, which is an essential point since vortices with high velocities can cause the resuspension of deposited particulate matter.

The work by Oliveira (2018) sought to evaluate gas-flow behavior in an industrial cycle-filter using the CFD tool. The software used was ANSYS Fluent v18.0. The simulations showed regions in the bags with filtration velocities three times greater than the design value, mainly due to the geometry similar to that of a cycle-filter funnel. Through this analysis, it was possible to associate the recurring premature failures in bags with the high filtration velocities in those regions, highlighting how the project's

design influences the performance of the process. In addition to the non-homogeneous flow distribution, a high-pressure gradient located in the cyclone was also observed. It was responsible for 75% of the total pressure drop generated by the equipment and low-pressure regions inside the cyclone, forming recirculation in these areas.

Lima (2019) developed a study on an existing fabric filter that suspected the non-uniformity of the gas flow distribution, due to the premature wear of some bags. For the simulation, ANSYS CFX v19.2 software was used. High velocities of the gas at the hopper's entrance and heterogeneous velocity distribution confirmed the suspicions. The author proposed two changes in the inlet design with deflectors aiming to standardize the flow through the reference case results. First, changing the lower part of the deflectors angle and addition of a deflector in the air inlet curve in the hopper. Second, in addition to the changes in the first alternative, there was a 15% reduction in the system flow. The first alternative showed more significant gains concerning the uniformity of the velocity and pressure field immediately below the bags.

Finally, Park et al. (2019) focused on understanding the pressure distribution and the filtration velocity on the surface of a single bag, since it is one of the dominant parameters that determine the pressure drop through a fabric filter. For this, the simulations were carried out in eight cases, combining four different lengths of long-bags filters (greater than 10 m) and two filtration velocities (1 m min^{-1} and 1,5 m min^{-1}). The numerical results regarding the pressure drop of a bag system were validated by comparison with experimental data and presented a maximum mean deviation equal to 8%. Experiments were carried out for 16 cases, combining four different lengths of long-bags filters and four different filtration velocities (1 m min^{-1}, 1,5 m min^{-1}, 2 m min^{-1}, and 3 m min^{-1}). The analysis showed that the filtration velocity is minimal at the bottom of the bag, but very high at the top, indicating that the upper section of the long-bag filter may deteriorate quicker than the lower part. In this way, the author developed an equation that can help to predict the initial pressure drop in long-bag filters with different heights, but with identical filtration characteristics.

Table 2: Summary of previous work about fabric filters.

	Damian et al. (2004)	**Nielsen, Skriver, and Castaño (2011)**	**Rocha et al. (2014) and Pereira et al. (2016)**	**Bernabé (2016)**	**Oliveira (2018)**	**Lima (2019)**	**Park et al. (2019)**
Objective	Improve the dedusting system performance in an asphalt industry through inlet design changes	Retrofit of pollution control equipment by optimizing the inlet flow distribution	Analyze how different inlet designs influences the air profile and filtration performance	Evaluate the gas flow characteristics inside an industrial fabric filter and propose design alternatives to improve operational efficiency	Evaluate the behavior of gas flow in an industrial cycle-filter to understand current problems associated to the filtering bags	Develop design solutions to improve the inlet flow distribution in a fabric filter	Understand the pressure and filtration velocity distribution on the surface of a single filtering bag
Solver	CFX 5.0	STAR-CD	ANSYS Fluent v13.0	ANSYS CFX v16.0	ANSYS Fluent v18.0	ANSYS CFX v19.2	ANSYS Fluent
Turbulence model	Standard k-ε	Standard k-ε	Realizable k-ε	Standard k-ε	RSM – Reynolds Stress Model	Realizable k-ε	Realizable k-ε
Fluid	Air at 115 ºC, incompressible and isothermal	Air 25 ºC, incompressible and isothermal	Air 25 ºC, incompressible and isothermal	Air 25 ºC, incompressible and isothermal	Air 25 ºC, incompressible and isothermal	Air 25 ºC, incompressible and isothermal	Air, incompressible and isothermal
Regime	Permanent	Permanent	Transient	Permanent	Transient	Permanent	Permanent
Mesh	Non structured	Not informed	Non structured	Non structured	Non structured	Non structured	Non structured
Inlet condition	Prescribed flow rate (40.000 $m^3 h^{-1}$)	Uniform inlet velocity	Inlet velocity (22,84 m s^{-1})	Prescribed flow rate	Inlet velocity (39,05 m s^{-1})	Inlet velocity (12,86 m s^{-1})	Prescribed flow rate
Outlet condition	Manometric pressure at the outlet (0 Pa)	Prescribed flow rate	Not informed	Manometric pressure at the outlet (0 Pa)	Manometric pressure at the outlet (0 Pa)	Manometric pressure at the outlet (0 Pa)	Atmospheric pressure at the outlet (1 atm)
Wall condition	No-slip (superficial rugoses of 500 µm)	No-slip	Not informed	No-slip	No-slip	No-slip	No-slip

3.4 PRECOATING OF THE FILTER MEDIUM

According to Andrade (2019), the filter medium is an essential factor for particle collection efficiency. The most common techniques for improving the filter medium are fabric material selection, superficial treatment of the bags, and precoating, which aim to reduce the pressure drop and the cleaning and maintenance cycles, increasing the bag's life, and, consequently, decreasing energy consumption and costs.

The fabric material selection must be adequate, considering its compatibility with the particulate matter that will be collected, and its characteristics and applications from each filtering process (BARNETT, 2000). Calendaring, Brushing, singeing, and chemical impregnation are ways of treating bags that provide better stability during filtration. Polytetrafluoroethylene (PTFE) membrane is another bags' treatment example that protects the fabric from abrasion, chemical attack, penetration of particles, high temperatures, and other problems. This technique can be applied over any material and promotes high filtration efficiency (99,99%) for fine particles (BARNETT, 2000). However, it has very high costs compared to other filter medium without this membrane (ANDRADE, 2019). For this reason, precoating is considered a promising alternative given its excellent results in increasing particle collection efficiency, simplicity, and lower cost (ANDRADE; SARTIM; AGUIAR, 2019).

Precoating consists of covering the new filter medium (nonwoven fabric) with particulate material, preventing the clogging of the bag by the penetration of sub micrometric particles. As represented in Figure 3, the content then assists in the dust cake initial formation, ensuring surface filtration, and preventing early saturation of the filter medium (ANDRADE, 2019). Furthermore, filters with precoating favor a better cake detachment from the surface, facilitating its cleaning (RAVERT, 2006).

Figure 3: Precoating's effect on the filter medium.

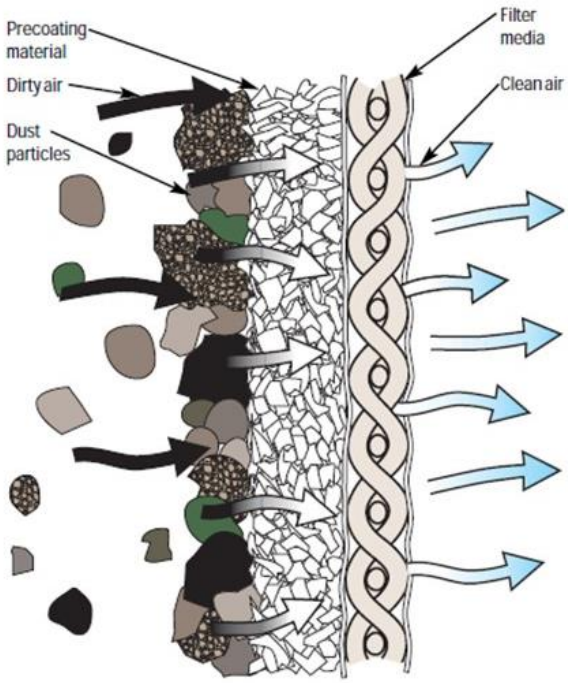

Source: Ravert (2006).

The selection of the precoating material is a fundamental aspect as it directly affects the filtration performance. Besides, the economic issue is also relevant since an industry requires large amounts of material to perform precoating on all equipment. Schiller, Hellmich, and Schmid (2016) highlight that the hydrated lime powder demonstrates proper functioning at affordable costs, plus Andrade, Sartim, and Aguiar (2019) point that this material is widely used in the steel industry's precoating of fabric filters. In addition to the choice of material, a premise for excellent precoating efficiency is that the powder distribution in the filter chamber and bags is uniform, as a result of homogeneous gas flow and velocity (SCHMIDT; LÖFFLER, 1990).

There is a lack of information in the literature regarding CFD simulation of particle injection in fabric filter for precoating reasons. Instead, CFD simulation of gas-solid two-phase flow in dedusting systems to improve gas and particle distribution and its operational efficiency is commonly found in control equipment such as cyclone separators. The works by Elsayed, Khairy and Lacor (2010); Ganegama, Bogodage and Leung (2015); and Song et al. (2017), for example, used more accurate and computational demanding numerical models in reason of their capability of better predicting the complex and swirling flow in the cyclone. Between these models, it is possible to list the k-ω SST and Reynold stress turbulence models to represent the swirling flow; and Discrete Random Walk (DRW) to serve the particle's motion in this

complex field. Additionally, other works focus on simulating the injection of hydrated lime particles in desulfurization systems (Flue Gas Desulfurization – FGD), aiming to reduce the exhausted fluid SO_2 content before collecting the particles with a dust control device. For instance, Gutiérrez Ortiz and Ollero (2008); Tang et al. (2013); and Marocco and Mora (2013) used the CFD to investigate the influence of modifications on the reactor's geometry and operational parameters in the gas-solid flow distribution to improve the SO_2 removal efficiency. For this purpose, the authors used turbulence and particle tracking models to simulate the fluid flow field and particle distribution, respectively. Moreover, a chemical species transport model between SO_2 and hydrated lime was also used to represent the desulfurization process. In the other hand, Adam, Everitt, and Riffat (1996); Zhang and Li (2008); De Almeida Santos et al. (2012); and Chang et al. (2019) applied the CFD tool to simulate the behavior of the particles in the flow stream in industrial ventilation ducts as part of the dedusting system. The authors proposed changes in the geometry and operational parameters to let the gas-solid flow more evenly distributed and thus enhance the dedusting efficiency.

What all these studies have in common is that they used CFD to understand the character of a gas-solid two-phase flow through the Euler-Lagrange approach, to optimize the process performance. In this approach, the flow field of the continuous phase (gas) was mathematically described. Then, the disperse phase (solid particles) was released into the simulated flow, and trajectories were tracked based on the prescribed equations of particle motion. The authors assumed that the presence of particles in the fluid does not affect the turbulent flow structure. This assumption is termed the one-way coupling assumption, referring to the fact that the fluid affects particle momentum, but the particles do not influence the momentum of the fluid (ANSYS, 2013).

Based on the advancement that the CFD has with the analysis of biphasic flows in dedusting systems, numerical simulation seems a powerful tool to evaluate the hydrated lime injections used for precoating. Therefore, this work intention is to contribute with the CFD investigation on gas-solid flow in ventilation systems, by simulating the gas flow distribution and the precoating particles in a fabric filter inlet duct, based on an existing industrial fabric filter design. Through the results, it will be possible to analyze the influence of the duct geometry in the airflow and the hydrated lime distribution pattern in the filter compartments inlet flow.

3.4.1 Correlated Works

Adam, Everitt, and Riffat (1996) provided evidence that CFD can be a useful tool for predicting the deposition of particles on duct walls. The author carried an experimental measurement of aerosol particles and tracer-gas in small-scale heating, ventilation, and air condition (HVAC) system to compare with a two-phase CFD model. In the experimental procedure, the particle deposition rate was calculated by measuring aerosol particle concentration at two measuring stations, one at the inlet and other at the outlet of the fitting's HVAC system. The particles were uniformly distributed in the cross-section slightly upstream of the first measuring station. Four distinct airflow rates were used (0,34; 0,42; 0,49; and 0,55 $m^3\ s^{-1}$) for eight different fittings: straight duct, reducer, single 90º bend, double 90º bend, 0º damper, 30º damper, 45º damper, and 60º damper. The authors used Fluent v4.2 software to simulate the gas-solid two-phase flow. Comparing the numerical results with the experimental data, they observed that the deposition rate was affected by the fitting used since the highest deposition rate occurred in the damper and the least in the reducer. Moreover, the increase in the flow rate produced a decrease in the deposition ratio. Nevertheless, for all the eight scenarios, the two results (numerical and experimental) were in close agreement, on which discrepancies occurred due to the five percent experimental error of the measurement and considerations made in the boundary conditions.

Zhang and Li (2008) developed another work to be helpful for particle deposition rates prediction in some environmental and industrial square ducts. The CFD simulation was conducted with the Fluent code and the DPM model to predict the deposition ratio of particles ranging from 10 to 20 μm in a horizontal square duct, with three different air velocities (3, 5, and 7 m s^{-1}). The numerical results were compared with experimental data available in the literature to show their agreement. It was visualized that dimensionless deposition rates of particles to the floor were higher than to the wall or the ceiling at different air velocities. Also, differences in deposition rates to the floor, wall, and ceiling decreased with increasing air velocities. The results showed that the deposition rate values decreased with friction velocity increase. To conclude, the authors pointed out that the deposition rate to the floor, wall, and ceiling was mainly dependent on two process variables, such as the magnitude of friction velocity and particle diameter.

De Almeida Santos et al. (2012) used the Fluent CFD code to develop the best retrofit solution to let the gas-solid two-phase flow as uniform as possible into a Primary Dedusting System duct of a basic oxygen furnace (BOF) converter and thus improve the dedusting performance. For this purpose, the authors simulated four scenarios: 1) current duct geometry based on data gathered with the device in operation; 2) increase of 2,2 mm in the inner duct diameter; 3) smoothing of the joints; 4) Extrapolation of dimensions to 2,9 mm.

In these simulations, two different heights of the duct skirt were considered, wholly closed to the converter's mouth and 100 mm above it. In the second option, the authors found that some amounts of environmental air at 40 ºC enter by the skirt; consequently, the oxygen of this air reacts with carbon monoxide from the furnace. Thus, a combustion model was used in this specific case to represent this chemical reaction. Further, a second simulation was made considering the heat exchange between the gas-solid flow and the cooling pipe system in the duct wall. The simulation of the stream with the skirt completely closed showed small variations in temperature between the four duct geometries. However, the air velocity profile suffered a significant influence on the design modifications, pointing out that the smoothed configuration promoted the best distribution of velocity along the section. Additionally, the smoothed condition contributed to reducing the particle impact under the surface of duct walls in a 180º curve, which is favorable for the duct service life. When the skirt was opened, the authors visualized that the numerical results coincided with the effects perceived in the real situation. For instance, the entrance air forced fumes to the center of the duct, resulting in the enhancement of particle collision in the hood's regions. Also, the air entrance caused an increase in the temperature due to post-combustion along the duct.

Another retrofit study was realized by Shi et al. (2017) to optimize a dedusting system efficiency built in a coal mine with the commercial Fluent software. During the coal mine operation, dust is generated from the digging and cutting location that is dispersed with airflow. Thus, the authors simulated three cases with different air duct allocations and dust concentration. Besides the three scenarios, the duct length was analyzed in distinct arrangements. For the second case, the authors used three distances (2, 3, and 5 m), and for the third one, more three lengths (2, 3, and 4 m). From the results, it was possible to observe that dust is not evenly distributed in space and time. Plus, a recirculation zone that coincided with higher dust concentration was

observed in scenario three. This same effect was not observed in configuration two. For this reason, the dedusting efficiency in this scenario was better than that with the absorbing air duct located in the middle of the heading roadway. Moreover, the dedusting efficiency decreased within the creasing distance between the air inlet and the duct location. Thus, the 2 m distance had the best dedusting capability, reaching up to 75,88% of the decrease in dust concentration in the mine.

Chang et al. (2019) carried out a CFD simulation to analyze the airflow characteristics and diesel particulate matter distributions in a development face in an underground mine in Westen Australia. This work is another example of particle tracking in indusial ventilation ducts, and also brings the concern about using this tool to prevent environmental issues. This investigation aimed to optimize the current exhaust ventilation system by simulating, besides the actual onsite scenario, two other ventilation designs with different duct lengths (5 m shorter and 5 m longer than baseline scenario) using the open-source software OpenFOAM. Plus, simulation results were used as parameter to compare with the local emission standards (0,1 mg/m³ and concentration limits (100 µg m^{-3}). The validation was made with onsite measurement data. The results confirmed that the current auxiliary exhaust ventilation system was unable to reduce the diesel particulate matter concentration effectively to meet the standards values. They visualized that the ventilation system with a duct length 5 m longer than the actual length provided a better particle dilution performance since the results showed that a vortex region became larger for shorter duct length, causing particle settling.

Table 3: Summary of previous work about simulation of particle in industrial ventilation ducts:

	Adam et al. (1996)	Zhang and Li (2008)	De Almeida Santos et al. (2012)	Shi et al. (2017)	Chang et al. (2019)
Objective	Compare experimental data of aerosol particles deposition rate in a small-scale HVAC system with numerical results	Contribute with particle deposition rate prediction in environmental and industrial square ducts.	Develop a design retrofit to let the gas-solid flow as uniform as possible into a Primary Dedusting System duct of a basic oxygen furnace (BOF) converter	Optimize a dedusting system model efficiency built in a coal mine heading roadway through design configuration proposals	Analyze the airflow characteristics and diesel particulate matter concentration distributions in an underground mine to optimize the current ventilation system
Solver	Fluent v4.2	Fluent	Fluent	Fluent	OpenFOAM
Turbulence model	k-ε model with calculated values of turbulence intensity and characteristic length	Realizable k-ε	k-ε model	Not informed	Standard k-ε with calculated values of turbulent kinetic energy and dissipation rate
Particle tracking model	DPM	DPM	DPM	DPM	Not informed
Continuous phase conditions	- Air at fixed temperature; - Four different prescribed inlet flow rates (0,34; 0,42; 0,49; and 0,55 $m^3 s^{-1}$); - Incompressible; - With heat exchange	- Air at fixed temperature - Three different inlet velocities (3, 5, and 7 m s^{-1}); - Incompressible, - Isothermal	- Gas at fixed temperature (1.700 ºC); - Prescribed flow rate (3.660 $Nm^3 min^{-1}$); - With heat exchange with cooling pipes at 80 ºC	- Air at prescribed flow rate (300$m^3 min^{-1}$) - Isothermal - Incompressible	- Air at 25 ºC; - Density of 1,206 kg m^{-3}; - Prescribed flow rate of 21,2 $m^3 s^{-1}$; - Incompressible; - Isothermal
Disperse phase conditions	- 100 oil smoke spherical and solid particles - Diameter of 2 µm; - Density of 865 kg m^{-3}; - Heat capacity of 200 J $kg K^{-1}$	- 40.000 spherical and solid particles injection at all three air velocities; - Diameters of with various diameters (10 - 200 µm); - Density of 1.500 kg m^{-3}	- Solid particles of fumes with mass flow rate of 1,69 kg s^{-1}; - Diameter of 100 µm;	- Solid particles with prescribed mass flow rate (0,008 kg s^{-1})	- Solid particles emitted at a flow rate of 1,219 10^{-6} kg s^{-1}; - Diameter of 78,7 10 nm; - Density of 1.770 kg m^{-3}; - Exhaust flow rate of 0,358 $m^3 s^{-3}$
Outlet conditions	Not informed	Outflow	Prescribed pressure of 2.500 mmCA	Prescribed air flow rate outlet (240 $m^3 min^{-1}$) does not contain dust	Atmospheric pressure (1 atm)
Regime	Permanent	Permanent	Permanent	Transient	Transient
Mesh	Not informed	Square elements – total mesh cells of 400	No-structured with 400.000 nodes	Tetrahedral elements – total mesh cells of 473.868	Tetrahedral and hexahedral elements – total mesh cells of 1,57 million
Wall condition	Particle deposit on duct walls after colliding with it, no reflection or resuspension permitted	No slip and particles deposit on duct walls after colliding with it, no reflection or resuspension permitted	Not adiabatic	Particles are reflected by the walls after colliding with it	No slip

3.5 MAIN POINTS OF THE LITERATURE OVERVIEW

The literature overview played an essential role in this work based on a real engineering case that sought to evaluate the influence of the duct system on the gas and particle flow in the fabric filter compartments inlet. It was possible to understand the important role that the pollution control technologies development has in reducing chronic effects on human health and meeting the atmospheric emissions limits.

It was possible, then, to understand the fabric filter operation, which are PM control equipment widely used in industries. The literature has shown that some premises are necessary for good filtration efficiency, such as the uniform distribution of gas flow in the equipment, in such a way that all fabric bags are subject to the same velocity and pressure. However, it was possible to observe in previous studies, that, in practice, this distribution ends up being heterogeneous, causing high pressure drop in the equipment and bags rupture, demanding high energy and maintenance costs. In this way, designers seek to make improvements in the fabric filter inlet duct geometry to meet this premise and increase filtration efficiency. Another practice widely used to improve filtration performance is the injection of hydrated lime into the filter inlet duct, which covers the fabric bags, preventing their corrosion and clogging of the pores.

With computational resources and software evolution, numerical simulation began to stand out as an engineering tool capable of analyzing fluid dynamics and their characteristics in complex problems. In this literature review several works that were found used Computational Fluid Dynamics (CFD) to understand the flow characteristics of fluids and particles in dedusting systems and PM control equipment. In addition, such works were able to analyze different scenarios of the same problem, proposing changes in geometry and operational parameters in order to find the scenario closest to the ideal. Such works served as motivation for this study, being the basis for the methodology followed and to perceive the analyzes that can be obtained using this tool.

4 METHODOLOGY

The work methodology initially consisted of collecting data of an existing fabric filter applied in a sinter plant. Then, the mathematical modeling parameters and the numerical method for the solution of the two-phase gas-solid flow were defined. Finally, the simulation results were evaluated with field measurements. Each of these steps is described in the following topics.

4.1 DATA COLLECTION

The first step was based on collecting information of the existing system, which is based on a real fabric filter operating in the Sinter Plant Primary Dedusting System presented in Figure 4.

Figure 4: Sinter Plant Primary Dedusting System.

The dedusting system is responsible for exhausting the gases and particles formed during the process and performing their treatment to meet the pollutant

concentrations emission limits in the stack. Large quantities of waste-gas are generated during the sintering process that contains dust and other environmentally harmful pollutants. According to Rizzo (2005), to produce the sinter, a mixture of fine iron ores and additives is agglomerated at high temperatures using coke as the combustion agent to produce a coarse grain product that is required by the blast furnace. As represented in Figure 5, in a conventional sintering process, 100% of the waste-gas exhausted from the sinter strand is directed to an air cleaning device and then released to the environment through the stacks. The heat energy contained in the gas and dust lost to the atmosphere in relatively high concentrations of pollutants such as SO_x, NO_x, CO_2 and CO are present in the environmental emissions (REMUS et al., 2013).

Figure 5: Sinter Plant.

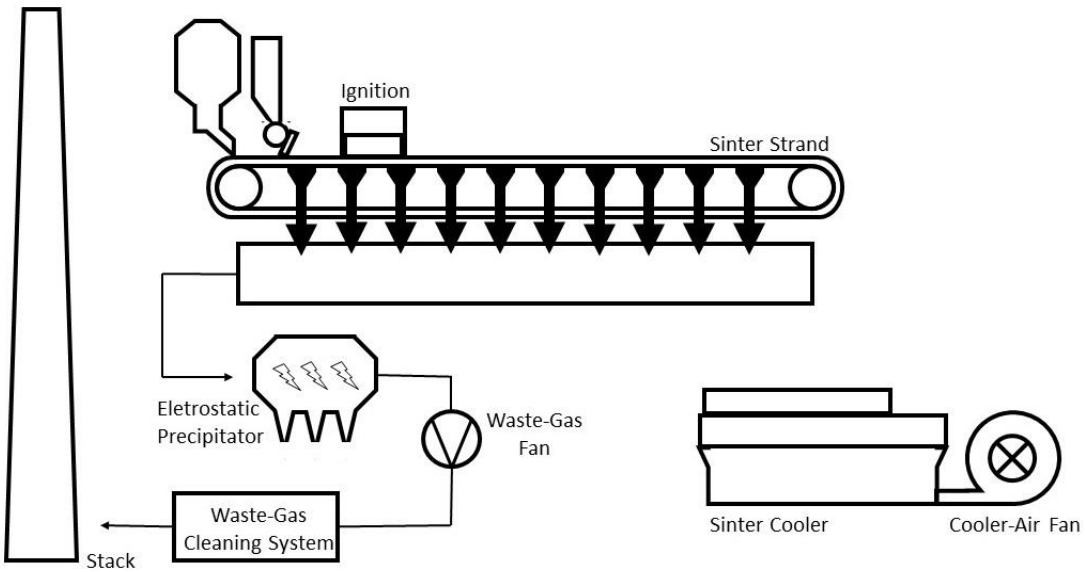

Source: Adapted from Remus et al. (2013).

Moreover, to enhance the dedusting system efficiency, continuous injections of hydrated lime ($Ca(OH)_2$) occurs at the gas inlet duct immediately upstream of the fabric filter. The alkaline material is dragged along with the gas stream to the fabric filter, accumulates on the surface of the bags, precoates, and prevents clogging of the pores of the fabric that protects them from corrosion (REMUS et al., 2013).

Information about the operational data of the fabric filter inlet duct are presented in Table 4.

Table 4: Operational characteristics of the fabric filter inlet duct.

Nº of compartments	8
Nº of bags	8.192
Bags length	8 m
Bags diameter	120 mm
PM mass flow in the duct inlets (mg/Nm³)	50
Gas volumetric flow in the inlet duct (Am³/h)	2.400.000
Inlet gas temperature (ºC)	150
Hydrated lime mass flow (kg s^{-1})	0,167

4.2 COMPUTATIONAL MODELING

Ansys Fluent is a tool that allows the simulation of fluid mechanics problems in any applications that involve gas flow, liquid flow, or heat transfer (ANSYS, 2017) by solving the conservation equations. In the present work, the commercial package Workbench was used, which aggregates the used softwares, such as SpaceClaim to draw the 3D geometry configuration, Fluent Meshing to construct the computational mesh, and Fluent v19 R2 used to solve the governing equations. This section 4.2 is divided by the steps performed in the computational modeling, represented by the flowchart shown in Figure 6.

Figure 6: Flowchart of the steps performed by the computational software used.

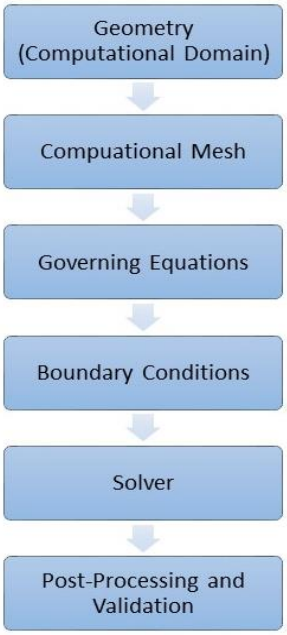

Source: Own authorship.

The post-processing and validation steps depend on the simulations' results; thus, this part of the methodologywill be presented in section 5.

4.2.1 Geometry

As shown in Figure 7, the fabric filter inlet duct, was designed to evenly distribute the off-gas from the sinter strand into sixteen outlets (eight on each side), on which two outlets correspond to one compartment, totalizing 4 compartments on each side. The two duct sects have 5 m diameter, which are connected at the outlet of two fans operating in parallel. Those two sects of duct converge into one main duct with 6,3 m diameter, and it is important to see that there are some guide vanes in order to make the flow more even distributed through this connection. Then, the main duct (straight segment), which is part of the fabric filter inlet duct, has15 m high and 77 m long.

Figure 7 also shows where the hydrated lime injections occur, which is released through two pipes of 500 mm located symmetrically on each duct sect, and were simplified by two planes in each side. It is worth mentioning that, there are some circular plates located in the main duct to improve hydrated lime particles distribution. However, the circular plates were not considered in the present work, so it is recommended to simulate them in future works to evaluate their position and influence on particles distribution.

Additionally, Figure 7 presents the bypass, which has the aim of diverting the gas flow directly to the stack when activated. This attachment is used when its stop is requested for inspection and maintenance.

Figure 7: Geometry of the fabric filter inlet duct

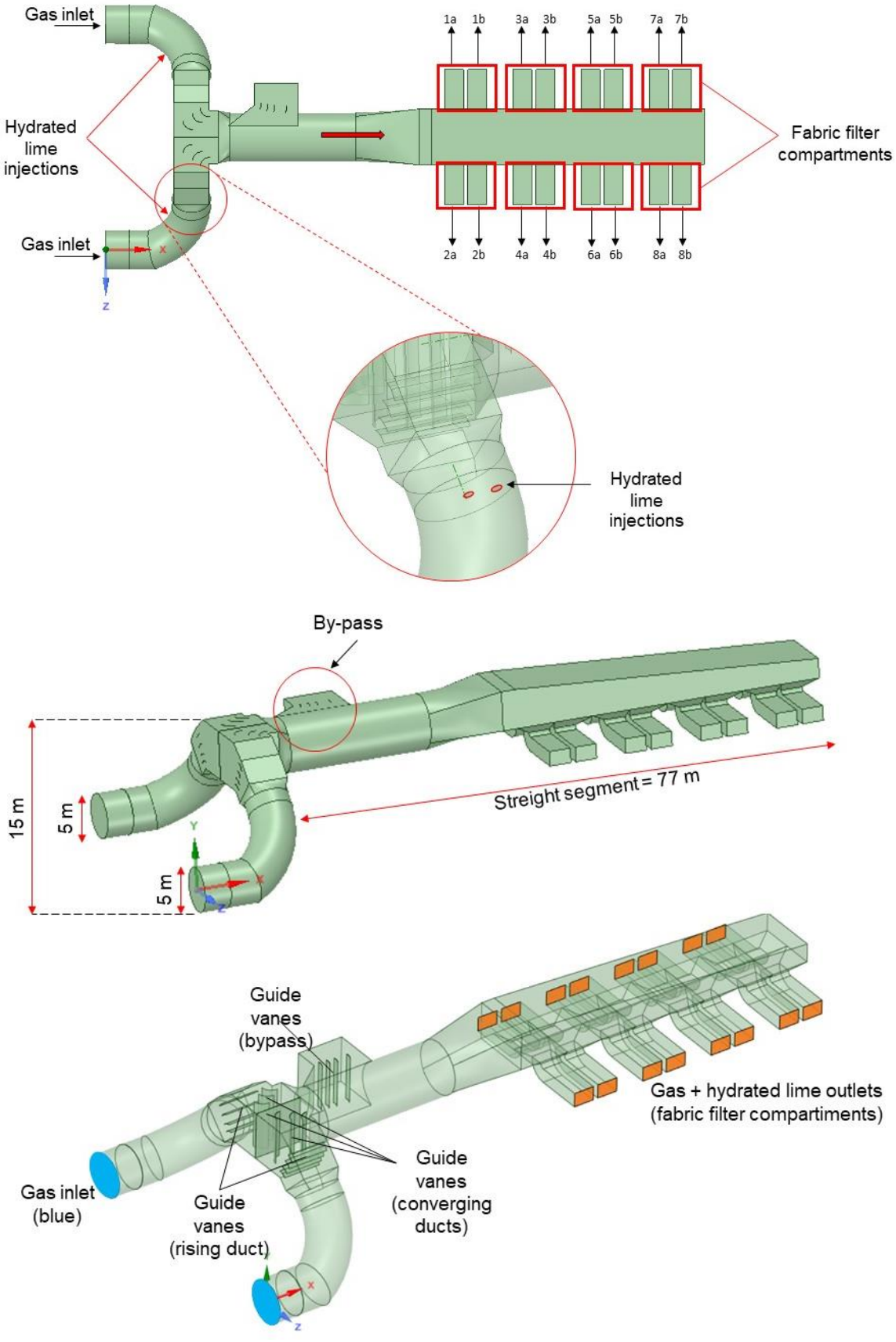

4.2.2 Computational Mesh

The computational grid (Figure 8) has approximately 6 million polyhedral elements. In the guide vanes and the ducts' wall, the mesh was refined with prismatic layers (inflation) to ensure the quality of the numerically produced results, that is, so that the flow physics is adequately represented.

A mesh test was made to verify the independence of the results according to the computational mesh's size. This analysis is essential to identify whether the computational mesh is negatively influencing the physical results of the model. The result of the mesh test will be presented in the Appendix A.

Figure 8: Computational mesh, with detail in the refinements.

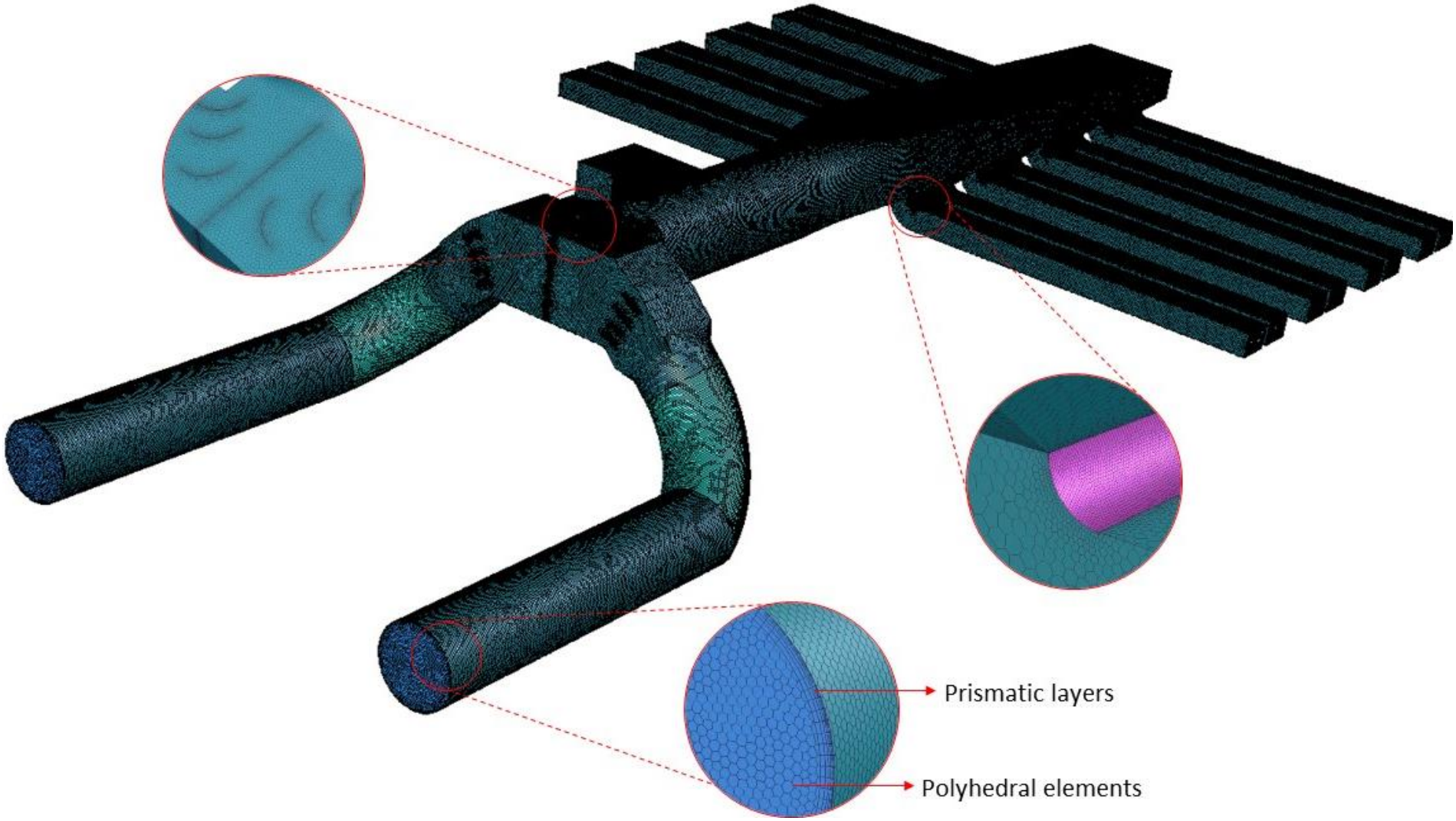

4.2.3 Problem Hypothesis

From the present problem interpretation, and based on the knowledge of the process and the fluid dynamics fundaments, it is possible to create hypotheses that will simplify the system. Such considerations and their justifications are shown in Table 5.

Table 5: Hypothesis adopted in this study.

Hypothesis	Justification
Permanent Flow	The gas and solid properties can be considered as constant in time
Incompressible Fluid	For Match number bigger than 0,3 the fluid is considered incompressible, since there is no heat exchange
Isothermal Conditions	The heat exchange between the two phases and the environment can be neglected
Fluid is a Continuous Medium	Any local property of the fluid remains unchanged
The hydrated lime are solid particles diluted in the continuous gas phase	The solid particles follows the main gas stream, thus gas-solid interaction can be neglected
Gravity influences only the solid disperse phase	The solid particles are dense so they are influenced by the gravitational force
No chemical reactions between the two phases (gas and solid) are considered	The objective study is to analyze the two-phase flow dynamics

With these hypothesis is possible to determine the methodology that will describe the problem. In this case, the problem will be numerically described, known as governing equations.

4.2.4 Governing Equations

The governing equations describe the physical and chemical phenomenon that occurs inside the system. According to the hypotheses, the flow is considered biphasic, so, the domain has a continuous phase (air at 25 ºC), and a discrete phase (solid particles of hydrated lime).

The mathematical models that describe biphasic flows are generally divided into Eulerian-Eulerian models and Eulerian-Lagrangian models, the differences of which are in the way the conservation equations are written for the two phases (Silva, 2006). In this case, the model used will be Eulerian-Lagrangian. In this approach, one

of the phases (gas) is modeled in Eulerian form, whose conservation equations are written for a control volume and the other (solid) in Lagrangian form, where its behavior is described along its trajectory. This approach is made when the second dispersed phase (solid) occupies a low fraction of the control volume even though the mass load is high (ANSYS, 2017).

According to Silva (2006), biphasic flows are classified by the coupling between the phases and can be considered one-way or two-way. During the movement of a particle in gas, it is possible to consider that it moves only due to the drag force that the fluid exerts on the particle and that this same force acts in the opposite direction in the fluid (two-way coupling). However, this force acting on the fluid may not be considered, resulting in a flow in one direction (one way). Furthermore, there are approaches in which it is necessary to consider the particle-gas interactions that generate disturbances in the other particles (triple-hand coupling) and particle-particle interactions (quadruple-hand coupling) (Norouzi et al. 2016). The way the phases interact with each other is influenced by two dimensionless values that help choose the most appropriate model for the simulation: the particle load (Equation 2) and the Stokes number (Equation 3).

$$\beta = \frac{\alpha_d \rho_d}{\alpha_c \rho_c} \tag{2}$$

Where α_d/α_c is the volumetric fraction between the dispersed and carrier phases and ρ_d/ρ_c is the material density rate calculated by the ratio between the density of the dispersed phase and the carrier phase. According to the Ansys manual (2017), the interaction degree between the phases can be divided into three categories according to the particle loading (β):

- For a very low value: the coupling between the phases is one-way.
- For an intermediate value: the coupling is two-way.
- For a high value: the coupling is triple hand or quadruple hand.

$$St = \frac{\tau_d}{\tau_s} \tag{3}$$

Where $\tau_d = \frac{\rho_d d_d^2}{18\mu_c}$ and τ_s is based on the length (L_s) and velocity (V_s) of the system: $\tau_s = \frac{L_s}{V_s}$. In this case:

- For St << 1: the particle will follow the movement of the gas flow (any approach can be used);
- For St> 1: the particles will move independently of the flow (only two-way approach or more) and;
- For St ~ 1 (again, any approach can be used).

Given that in the current system, it was obtained β = 2,3 10^{-4} and St = 6,42 10^{-3}, the Euler-Lagrange model will be approached, where the gas fluid will be treated in the Eulerian form and the particles of hydrated lime in the Lagrangian form.

4.2.4.1 Continuous Gas Phase

The gas phase is described by the continuous phase transport equations: by macroscopic properties, such as velocity, pressure, temperature, density, and their derivatives in time and space. Thus, governing equations of fluid flow represent mathematical statements of the conservation principles of physics following the hypotheses that the fluid is a continuous medium (see in section 4.2.3):

- Mass Conservation Principle: the mass of a fluid inside a system is conserved;
- Momentum Conservation Principle: a momentum rate of change is equal to the sum of forces in a fluid particle (Newton Second Law).

The equations of mass conservation, momentum, and turbulent kinetic energy solved to the gas phase are detailed by Versteeg and Malalasekera (2007). The mass conservation equation is given by Equation 4.

$$\frac{\partial \rho}{\partial t} + \frac{\partial (\rho u_i)}{\partial x_i} = 0 \qquad (4)$$

Where, u_i is the flow velocity (m s^{-1}), t the time (s) and ρ is the specific mass of the gas (kg m^{-3}). The Equation 4 is the tree-dimensional and unsteady continuity equation at a point in a compressible fluid. Although, in the present model, the fluid is considered incompressible and the flow is permanent, so that the continuity equation can be simplified to Equation 5.

$$\frac{\partial(u_i)}{\partial x_i} = 0 \tag{5}$$

From Newton Second Law, the momentum equation represents the equilibrium of body and surface forces acting on the fluid particle, and defined by Equation 6.

$$\frac{\partial(\rho u_i)}{\partial t} + \frac{\partial(\rho u_i u_j)}{\partial x_j} = -\frac{\partial(p\delta_{ij})}{\partial x_i} + \frac{\partial \tau_{ij}}{\partial x_j} + \rho g_i \delta_{3i} \tag{6}$$

Where p is the static pressure (kg m^{-1} s^{-2}). For a Newtonian fluid, τ_{ij} is proportional to the shear strain rate, expressed by Equation 7.

$$\tau_{ij} = \mu\left(\frac{\partial u_i}{\partial x_j} + \frac{\partial u_j}{\partial x_i}\right) - \frac{2}{3}\mu\left(\frac{\partial u_j}{\partial x_j}\right)\delta_{ij} \tag{7}$$

Since δ_{ij} is the Kronecker delta, where δ_{ij}= 1 if $i = j$ and δ_{ij}= 0 if $i \neq j$, and μ is the dynamic viscosity (property of the fluid). When Equation 7 is substituted in Equation 6, we have the momentum equation in terms of deformation rate, also known as Navier-Stokes equation. This expression ca be simplified by the hypotheses that the fluid is incompressible and the flow permanent, generating the Equation 8.

$$\frac{\partial(\rho u_i u_j)}{\partial x_j} = -\frac{\partial p}{\partial x_i} + \frac{\partial}{\partial x_j}\left[\mu\left(\frac{\partial u_i}{\partial x_j} + \frac{\partial u_j}{\partial x_i}\right)\right] + \rho g_i \delta_{3i} \tag{8}$$

The conservation equations, even after simplifications, do not have analytical solutions, so it is necessary to perform methods for numerical solutions that will be discussed in Section 4.2.6.

4.2.4.1.1 Turbulence Modeling

According to Malalasekera (1995), turbulent flows are characterized by high Reynolds number, differently from laminar flows. The Reynolds number is a non-dimensional value used for intern flows, which indicates if the flow is laminar or turbulent. The flows will generally be laminar for Re ≤ 2.300 and turbulent for Re> 4.000 (FOX; MCDONALD; PRITCHARD, 2014). The numeric expression is indicated in Equation 9.

$$Re = \frac{\rho v D}{\mu} \tag{9}$$

Where v is the mean fluid velocity, D is the duct diameter, ρ is the fluid specific mass, and μ is the fluid dynamic viscosity. Through the data given in this section 4, the Reynolds number calculated for the simulated domain was bigger than 4.000, indicating that this system regards a turbulent flow.

The turbulent fluctuations in the flow velocity field cause the amounts transported to mix, such as momentum and energy, causing the values of the transported quantities to fluctuate as well. Thus, to predict the turbulence effects, it is necessary to use a turbulence model, which are divided according to Versteeg and Malalasekera (2007).

- Turbulence models for Reynolds Mean Equations (RANS: Reynolds-averaged Navier-Stokes): attention is given to the mean flow and the effects of turbulence on the properties of the mean flow. The computational resources required to obtain reasonably accurate results are modest, so they have been the main method for calculating flow in the last decades.
- Large Eddy Simulation (LES): it is an intermediate form of calculating turbulence, which tracks the behavior of larger scale vortices. Therefore, this method solves the Navier-Stokes equations in a transient way for the large scale vortices and rejects the small scale vortices, modeled in the mean flow. The resolution of these effects

requires a greater computational effort and, currently, it is being applied to problems with more complex geometries.

- Direct Numerical Simulation (DNS): This method calculates both the mean flow and all turbulent velocities fluctuations. Simulations with this model require a high computational cost and, therefore, it is not yet used in industrial applications.

In this work, the effects of turbulence were modeled using the RANS method requiring reduced computational cost, obtained through the representation of the properties involved in the model according to their average and their fluctuations. This concept is also known as Reynolds decomposition, as represented by Equation 10.

$$u(t) = \bar{u} + u'(t) \tag{10}$$

Where $u(t)$ is the instantaneous velocity in t, $\bar{u}$ is the average velocity and $u'(t)$ is the fluctuation of the velocity at the time t. In this way, the governing equations (continuity and Navier-Stokes) are represented by replacing the instantaneous values with the average values and their fluctuations, according to Equation 11 and Equation 12

$$\frac{\partial(\bar{u}_i)}{\partial x_i} = 0 \tag{11}$$

$$\frac{\partial(\rho \bar{u}_i \bar{u}_j)}{\partial x_j} = -\frac{\partial p}{\partial x_i} + \frac{\partial}{\partial x_j}\left[\mu\left(\frac{\partial \bar{u}_i}{\partial x_j} + \frac{\partial \bar{u}_j}{\partial x_i}\right) - \rho\overline{u'_\iota u'_\jmath}\right] - \rho g_i \tag{12}$$

The term $-\rho\overline{u'_\iota u'_\jmath}$ appears in Equation 12 due to the interactions between the various turbulent fluctuations, and is called Reynolds stresses. Boussinesq proposed, in 1877, that the Reynolds stresses are proportional to the mean flow deformation rates (VERSTEEG; MALALASEKERA, 2007). Therefore, they can be expressed as Equation 13.

$$-\rho\overline{u'_\iota u'_\jmath} = \mu_t\left(\frac{\partial \bar{u}_i}{\partial x_j} + \frac{\partial \bar{u}_j}{\partial x_i}\right) - \frac{2}{3}\rho k \delta_{ij} \tag{13}$$

Where $k = \frac{1}{2}\left(\overline{u'^2} + \overline{v'^2} + \overline{w'^2}\right)$ is the turbulent kinetic energy and μ_τ is the tubulent viscosity, property of the flow that must be modeled. Thus, Equation 14 is generated by replacing Equation 13 in Equation 12.

$$\frac{\partial(\rho\bar{u}_i\bar{u}_j)}{\partial x_j} = -\frac{\partial p}{\partial x_i} + \frac{\partial}{\partial x_j}\left[\mu_{eff}\left(\frac{\partial\bar{u}_i}{\partial x_j} + \frac{\partial\bar{u}_j}{\partial x_i}\right) - \frac{2}{3}\rho k\,\delta_{ij}\right] - \rho g_i \tag{14}$$

Where $\mu_{eff} = \mu + \mu_t$ is the effective viscosity.

For the modeling of turbulent viscosity (μ_τ), the $k{-}\varepsilon$ model initially developed by Launder (1974) has two equations: one for k, the turbulent kinetic energy, and one for ε, the dissipation rate of the turbulent kinetic energy. Thus, turbulent viscosity is defined as Equation 15.

$$\mu_t = C_\mu \frac{pk^2}{\varepsilon} \tag{15}$$

Where $C_\mu$is an adjustment constant.

According to Malalasekera (1995), the RANS $k{-}\varepsilon$ turbulence model is the simplest and most widely used and validated turbulence model. It promotes robustness, economy, and reasonable accuracy for a broad spectrum of turbulent flows. The model is based on the turbulent scales of high Reynolds numbers, so it is necessary in the free flow region, but it does not obtain good results in regions close to the boundary layer and in rotating flows. Additionally, improvements have been made to the standard model, such as the $k-\varepsilon$ RNG and $k-\varepsilon$ Realizable models (CABLE, 2009).

The realizable $k{-}\varepsilon$ model proposed by (SHIH et al., 1994) is, among the variations of the k-ε models, the most recent and presents a main difference when compared with the standard model: C_μ is no longer constant, promoting higher sensitivity of the model to variations in flow and turbulence. This consideration is not met by any of the other two $k{-}\varepsilon$ models (standard and RNG), making the Realizable model more accurate in predicting flows, as in separate flows and complex secondary flows (CABLE, 2009).

Given the presence of curves and deflectors in the geometry of this work adds to the Standard model's disadvantages in recirculating flow and boundary layer, the Realizable k-ε model was chosen, where the effect of mean rotation in the turbulent viscosity could be considered (ANSYS, 2017). Thus, by using the k–ε Realizable turbulence model the governing equations became as Equation 16 and Equation 17.

$$\frac{\partial}{\partial x_j}(\rho k u_j) = \frac{\partial}{\partial x_j}\left[\left(\mu + \frac{\mu_t \partial k}{\sigma_k \partial x}\right)\frac{\partial k}{\partial x_j}\right] + G_k + G_b - \rho\varepsilon - Y_M + S_k \quad (16)$$

$$\frac{\partial}{\partial x_j}(\rho \varepsilon u_j) = \frac{\partial}{\partial x_j}\left[\left(\mu + \frac{\mu_t}{\sigma_\varepsilon}\right)\frac{\partial \varepsilon}{\partial x_j}\right] + \rho C_1 S\varepsilon - \rho C_2 \frac{\varepsilon^2}{k + \sqrt{v\varepsilon}} + C_1 \varepsilon \frac{\varepsilon}{k} C_3 \varepsilon G_b + S_\varepsilon \quad (17)$$

Where G_k is the production of kinetic energy by buoyant forces; ε the rate of kinetic energy dissipation; G_b the production of turbulent kinetic energy due to fluctuation; Y_M the fluctuating expansion in turbulent compressibility that contributes to the rate of dissipation; S_ε and S_k are source terms; σ_k and σ_ε are the Prandtl numbers for turbulent kinetic energy and their dissipation; and C_1, C_2 and C_3 are constants determined experimentally.

4.2.4.2 Dispersed Phase – Hydrated Lime

Once the gas velocity field is known, the hydrated lime particle injections are computed. The dispersed solid phase is described by the Disperse Phase Model (DPM) available in the Fluent software. The model uses the Lagrangian approach by tracking a large number of particles, called parcels, through the computational domain. A parcel is commonly identified as a discrete element (ANSYS, 2017). It is assumed that the parcel of particles moves through the computational domain with the same properties (velocity, density, and pressure) as a single physical particle.

The continuity and momentum equations for a single nonrotating parcel take are described in Equation 18 and Equation 19.

$$\frac{dx_p}{dt} = u_p \quad (18)$$

$$m_p \frac{du_p}{dt} = \frac{1}{2}\rho C_d |u - u_p|(u - u_p) A_p + m_p g \quad (19)$$

The hydrated lime particles were considered as a solid and spherical material. Thus, the drag force acting in the particles is represented by the coefficient C_d, and is evaluated through the Morsi and Alexander correlation (MORSI; ALEXANDER, 1972). Considering that gravitational settling is one of the main mechanisms of particle deposition in turbulent duct flows (LU; WANG, 2019), some particles with bigger diameter can deposit in the duct walls, thus, the gravitational force acting in the solid particle is also considered in Equation 19.

When a particle hits the duct walls, its trajectory is modified by considering an ideal reflection, which means that the tangential velocity component remains unchanged in magnitude and direction. In contrast, the normal velocity component changes its direction by and angle of 180º. This simplified particle-wall interaction model does not influence the flow field of the gas because of the momentum de-coupling between the two phases. Moreover, the volume fraction of the dispersed phase is meager, and only a few particles hit the walls. Therefore, the accuracy of the solution obtained does not depend on the above hypothesis.

Discrete Random Walk model (DRW) or “eddy lifetime” was used to model the turbulent dispersion of particles. This is a stochastic tracking method available in the Fluent software to determine the instantaneous fluid phase velocity, instead of using its mean velocity to predict the dispersion of the particles due to turbulence (ANSYS, 2017).

4.2.5 Boundary Conditions

The boundary conditions required for the flow solution include the gas velocity inlet, the hydrated lime mass flow inlet, the pressure manometric outlet, and the non-slip wall condition. Such circumstances are described in Table 6.

Table 6: Boundary conditions used in the work.

Boundary	Type	Value
Gas phase inlet	Velocity inlet	16,928 m s^{-1}
Solid phase inlet	Mass flow inlet	0,167 kg s^{-1}
Solid phase transport air inlet	Velocity inlet	12 m s^{-1}
Outlet	Pressure outlet	0 Pa (manometric)
Duct and deflectors walls	No slip condition for the gas and ideal reflection for the solid	V = 0
Fluid	Air ideal gas	T = 25 ºC ρ = 0,83 kg m^{-3}
Solid particle	Hydrated lime	ρ = 2.210 kg m^{-3} ∅ = 0,77 to 243,427 µm

As the hydrated lime particles injected in the original duct do not have a homogeneously distributed diameter, it was necessary to add several injections with different diameters into the domain to get as close to reality as possible. Figure 9 presents the granulometric distribution graph of the hydrated lime used in the system, and Table 7 shows the injection parcels added to the numerical model.

Figure 9: Hydrated lime's particle size distribution.

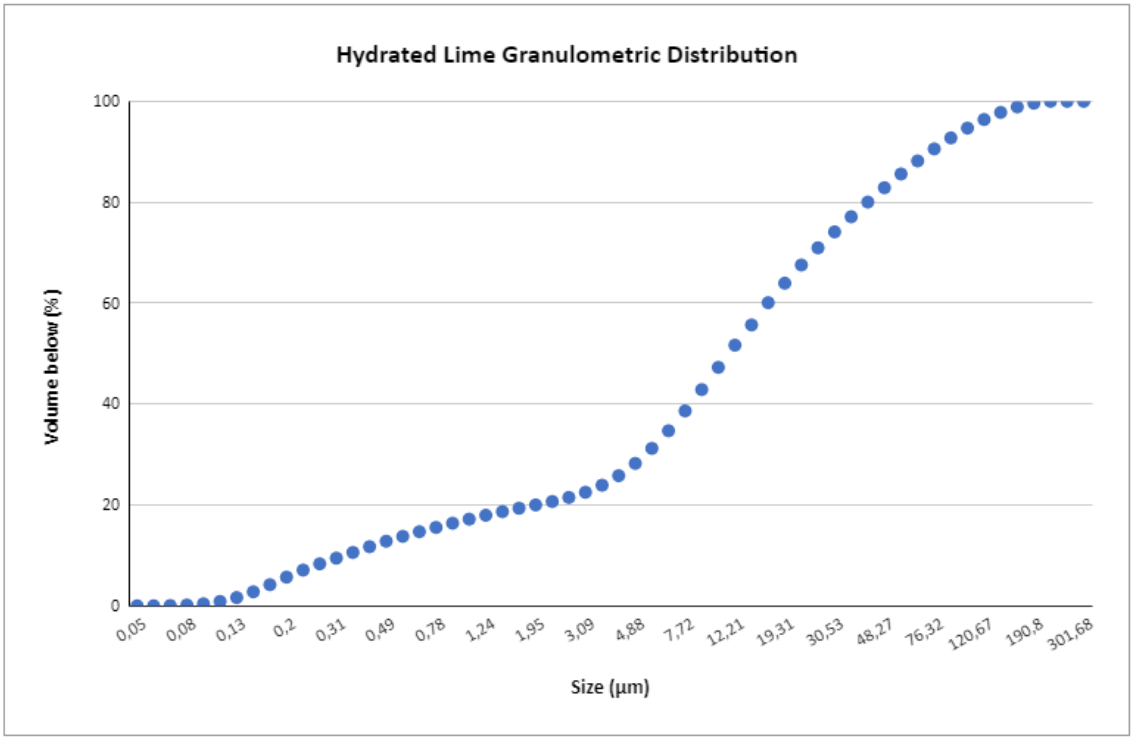

Source: Data given by the steel industry.

Table 7: Hydrated lime injections into the computational domain.

Injection	Diameter (um)	Parcel (%)	Mass flow (kg s^{-1})
1	0.077	0.252	0.0004
2	0.192	4.702	0.008
3	0.472	7.217	0.012
4	1.185	5.342	0.009
5	2.960	4.885	0.008
6	7.400	14.752	0.025
7	18.500	24.502	0.041
8	46.221	19.670	0.033
9	115.638	13.862	0.023
10	243.427	4.978	0.008

4.2.6 Governing Equation Solution Method (Solver)

Traditional methods for numerically solving the governing differential equations are the Finite Difference (FDM), the Finite Volumes (FVM), and the Finite Elements (FEM) (MALISKA, 2004). In this work, the Ansys Fluent software (v19 R2) uses the Finite Volume Method.

According to Versteeg and Malalasekera (2007), in the FMV method the domain is divided into control volumes, each containing a nodal point (in the centroid). Each volume's faces are positioned between two nodes, so each node is surrounded by other control volumes. Subsequently, in the discretization phase, the FVM integrates the governing equations in each control volume, obtaining a discretized equation at each nodal point. From the discretized equations, there is a system of equations to be solved.

As the present study is an incompressible flow, the density is constant, and, by definition, it is not dependent on pressure. However, when calculating the flow, it is also desired to obtain the pressure field as part of the solution. Thus, it is necessary to use an algorithm to couple the equation system, involving pressure in the mass conservation equation, known as pressure-velocity coupling. In this study, the pressure-based solver was used, with the Coupled approach algorithm resolution. This method solves the momentum and pressure-based continuity equations and offers some advantages over the non-coupled or segregated approach (SIMPLE and SIMPLEC). It obtains a robust and efficient single-phase implementation for steady-state flows, with superior performance compared to them (ANSYS, 2017).

The Ansys Fluent software stores the discrete values of a scalar variable in the center of the cells. Diffusive terms are calculated using the central difference method and always with second-order precision. However, for convection terms, property values are required on faces, so they need to be interpolated. For this, an upwind scheme is used (ANSYS, 2017). The term upwind means that the value of the property on the face, φ_f, is derived from the quantities of the upstream cell, relative to the direction of normal velocity. When a first order precision (FOU - First Order Upwind Scheme) is sufficient, the quantities on the faces of the cells are obtained assuming that each variable's central values are an average value in the cell, equal throughout the control volume. In this way, the quantity on the face is identical to the quantity in

the center of the cell ($\varphi = \varphi_f$). When second-order precision is desired (SOU - Second-Order Upwind Scheme), the quantities on the faces of the cells are calculated using a multidimensional linear reconstruction approach. Thus, higher-order precision is achieved on the cells' faces from expansion by the cells' center solution Taylor series (ANSYS, 2017), as shown in Equation 20:

$$\varphi_{f,SOU} = \varphi + \nabla\varphi.\vec{r} \tag{20}$$

Where φ and $+\nabla\varphi$ are, respectively, the value in the center of the cell and its gradient in the upstream cell, and $\vec{r}$ is the displacement vector of the cell upstream to the centroid of the analyzed cell. In this work, for the discretization of the pressure gradient, the Second-Order scheme was adopted. In the case of continuity and momentum equations, the second order upwind scheme (SOU) was also used. Nevertheless, for the k and ε equations, the first order upwind scheme (FOU) was used.

The simulation was carried out in parallel processing divided into eight cores with 128 GB of available RAM, and 2.000 interactions were performed, totalizing 3 hours and 20 minutes of duration.

Finally, the convergence criteria used was RMS (root mean square), a minimum residual value of $1x10^{-4}$, which is considered reasonable for many engineering applications (ANSYS, 2017). Table 8 shows, in summary, the modeling used to perform the simulation, according to the data presented in Section 4.

Table 8: Simulation modeling summary.

Turbulence model (gas continuous phase)	Realizable $k-\varepsilon$
Particle Tracking model (solid dispersed phase)	Discrete Phase Model (DPM)
Wall function	Scalable
Pressure-velocity coupling	Coupled
∇P discretization	Second-order
Advection schemes	
Continuity equation	Second-Order Upwind
Momentum equation	Second-Order Upwind
k and ε equations	First-Order Upwind

5 RESULTS

In this section, the results obtained through the numerical simulations will be presented. Section 5.1 presents the analysis of gas characteristics in the computational domain. In this analysis, the air streamlines, velocity, and pressure distribution are observed along with the ducts and outlets. Subsequently, section 5.2 analyzes the distribution of hydrated lime injected into the duct. The trajectory of the solid particles will be investigated, as well as the velocity, mass flow, and residence time.

5.1 FLUID FLOW BEHAVIOR

The airflow behavior profoundly influences the hydrated lime dispersion and concentration. Also, in areas with vortex, its position and size play significant roles in affecting the particle settling. Thus, it is crucial to understand the airflow characteristics under the existing duct work first so them the particles can be analyzed.

The average velocity for particles transport in a duct system recommended for industrial ventilation cases is in the range of 17 to 20 m/s (ACGIH, 2019a). Therefore, very low velocities zones can be susceptible to particle settling, while very high areas can increase the friction in the duct walls. In this logic, Figure 10 shows the air flow streamlines in the fabric filter inlet duct and vortex areas formation with low velocity (bellow 8 m/s), that can potentially cause hydrated lime settling.

As can be seen, the air flow pattern is strongly affected when it meets the bypass, forming there a recirculation zone with low velocity. In the zoom, another low-velocity recirculation region is visible in outlets 5b and 7b, due to the combined effect when the air flow in the main direction meets the air reflected by the wall.

Another interesting result in this Figure, is that the streamlines are heterogeneously distributed between the duct outlets. For instance, outlets 1b and 2b apparently have no streamlines, so, the fabric filter compartments are not operating in the same conditions. As the airflow is responsible for carrying the hydrated lime particles, the compartments are probably not getting the same amount of particles. The following discussions will investigate this result with more details in order to understand what seems to cause it.

Figure 10: Current duct streamlines.

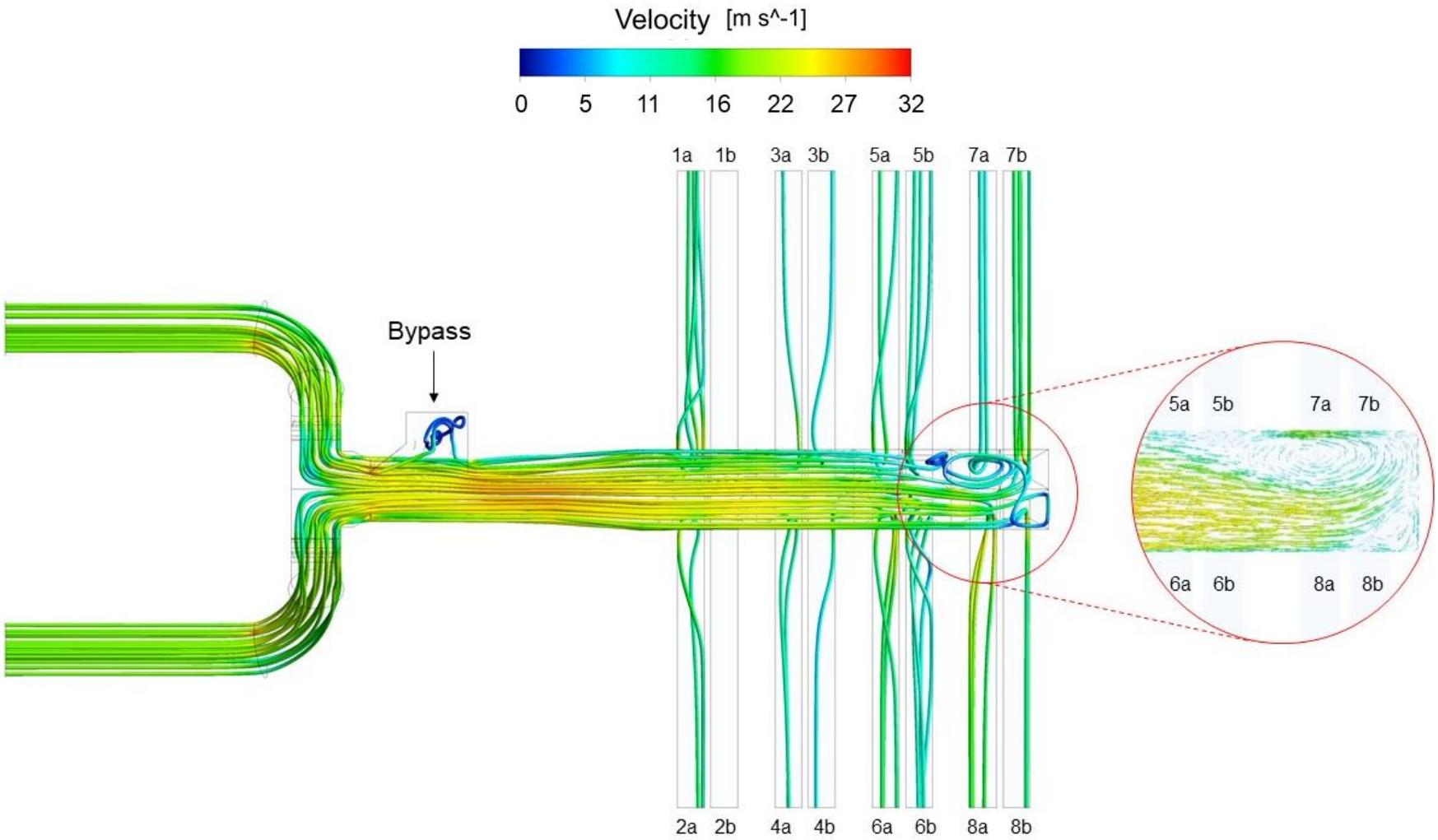

To analyze the bypass influence on the flow pattern, a simulation of the same geometry was performed, however, without the bypass (Figure 12). Plus, this geometry had the same mesh conditions. It is possible to perceive greater homogeneity and symmetry in the air flow distribution at the straight segment. In the meanwhile, outlets 1b and 2b again seem to get no streamlines.

Additionally, the recirculation region observed in the zoom in Figure 10 is not present in this scenario. The only recirculation visible in this case is the one at the end of the straight segment, which was generated by the wall reflection.

Figure 11: Streamlines of the duct without the bypass.

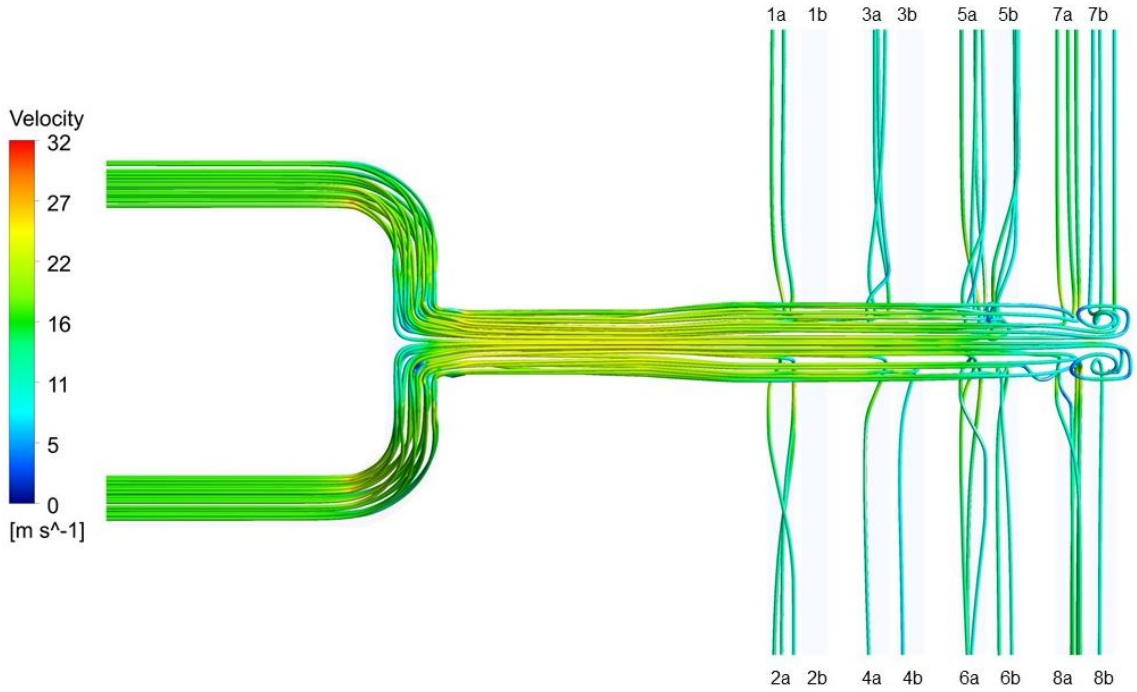

As the inlet flow distribution uniformity is a premise to guarantee the filtration process efficiency, in Figure 12 is possible to analyze the average flow velocities at the fabric filter compartments inlet, that correspond to the duct outlets.

In the existing design scenario (a), there is a considerable difference in the average velocity distribution between the compartments. Considering that the mean velocity is about 10 m/s, the compartments 1 and 2 have the lower values (around 7 m/s). These compartments are exactly those that contemplate outlets 1b and 2b that apparently had no streamlines in Figure 10. However, the compartments on opposite sides showed very close values, with the exception of compartments 7 and 8, possibly due to the low-velocity and recirculation region between exits 5b and 7b shown in the zoom in Figure 10.

In the hypothetical scenario without the bypass (b), as expected, the compartment inlet average velocities show small variation. These results demonstrate that the bypass actually causes a disturbance in the flow pattern causing heterogeneity in the distribution of the average velocity in the fabric filter compartments.

Figure 12: Average velocity at each compartment inlet of the filter for the existing duct (a) and the hypothetical duct without the bypass (b).

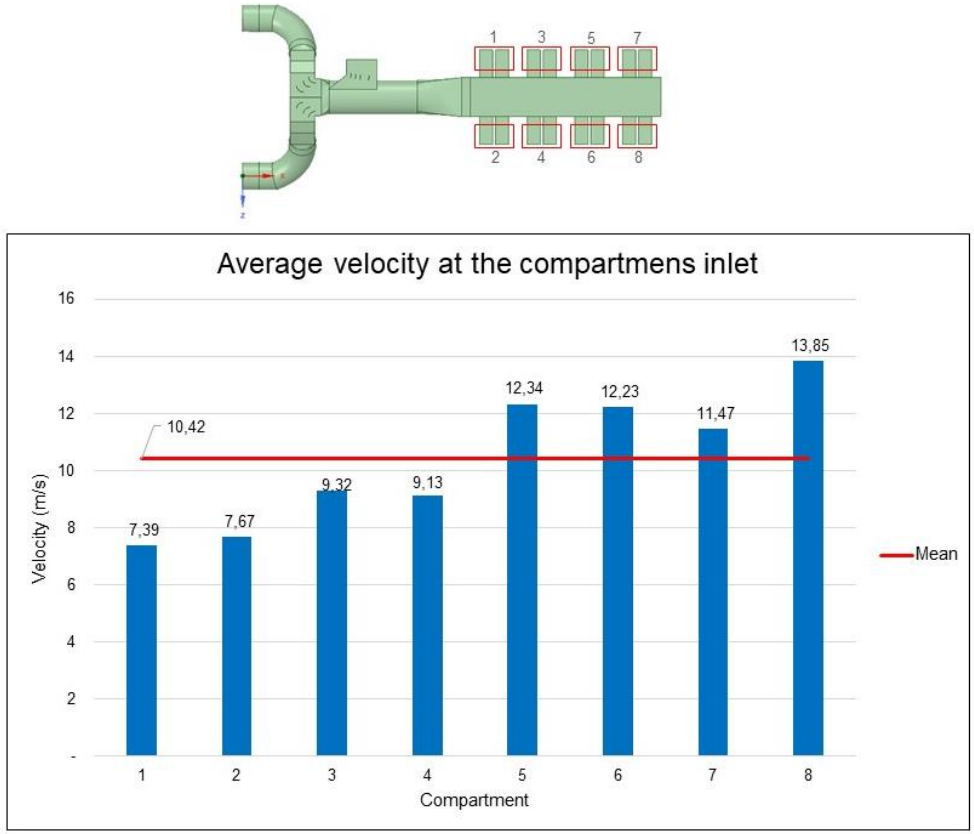

(a)

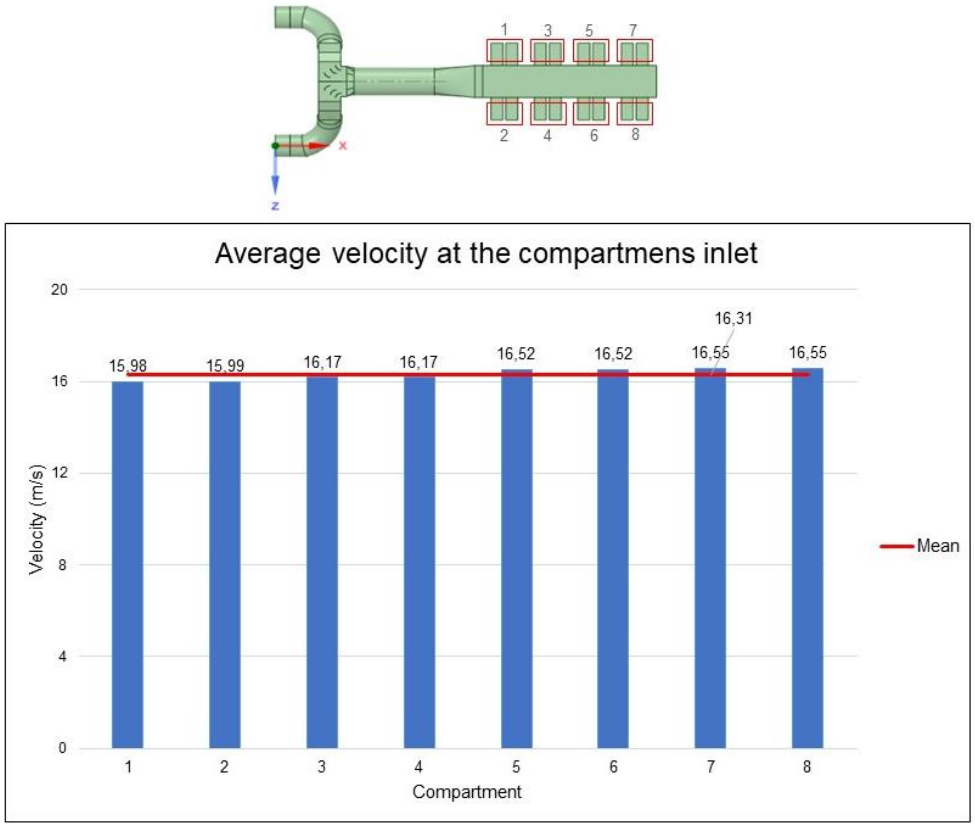

(b)

The velocity distribution at the filter inlet duct can be seen in Figure 13, which shows the velocity field plotted in the horizontal planes colored in red for both scenarios.

In the existing design scenario (a), the flow separates from the wall when it meets the bypass. Consequently, given the recirculation zone in the bypass, the flow gets squeezed on the opposite side of the duct and accelerates there, reaching velocities above 20 m/s. Such regions are usually points that need attention in terms of maintenance since, due to these high velocities above the recommended by ACGIH (2019a), there is a greater friction of the particles contained in the flow with the wall and, consequently, a greater risk of wear, such as holes in the structure.

It is observed in Figure 13a that the compartments in opposite sides present similar behavior, such as observed in Figure 12a for all compartments, except the compartments 7 and 8. The recirculating region with low velocity between outlets 5b and 7b, also seen in Figure 10, is apparently the cause why compartment 7 presented a lower velocity than the compartment 8 found in Figure 12a.

In the hypothetical scenario without the bypass (b), the velocity field is totally symmetric in relation to the AB line. It is possible to observe that as the flow enters the fabric filter compartments, it loses velocity along the straight segment. However, in both scenarios outlets 1b and 2b stands out with velocity below the others compartments (under 8 m/s). These outlets are the same ones that seemed to have no streamlines in Figures 12 (existing duct scenario) and 13 (hypothetical scenario without bypass). Therefore, this result suggest that other configuration of the duct work geometry is causing this discrepancy in outlets 1b and 2b, but not necessarily due to the bypass presence. This result indicates that the existing duct promotes this non uniform flow.

Figure 13: Velocity distribution at half the height of the inlet duct for the existing (a) and hypothetical without the bypass (b) scenarios.

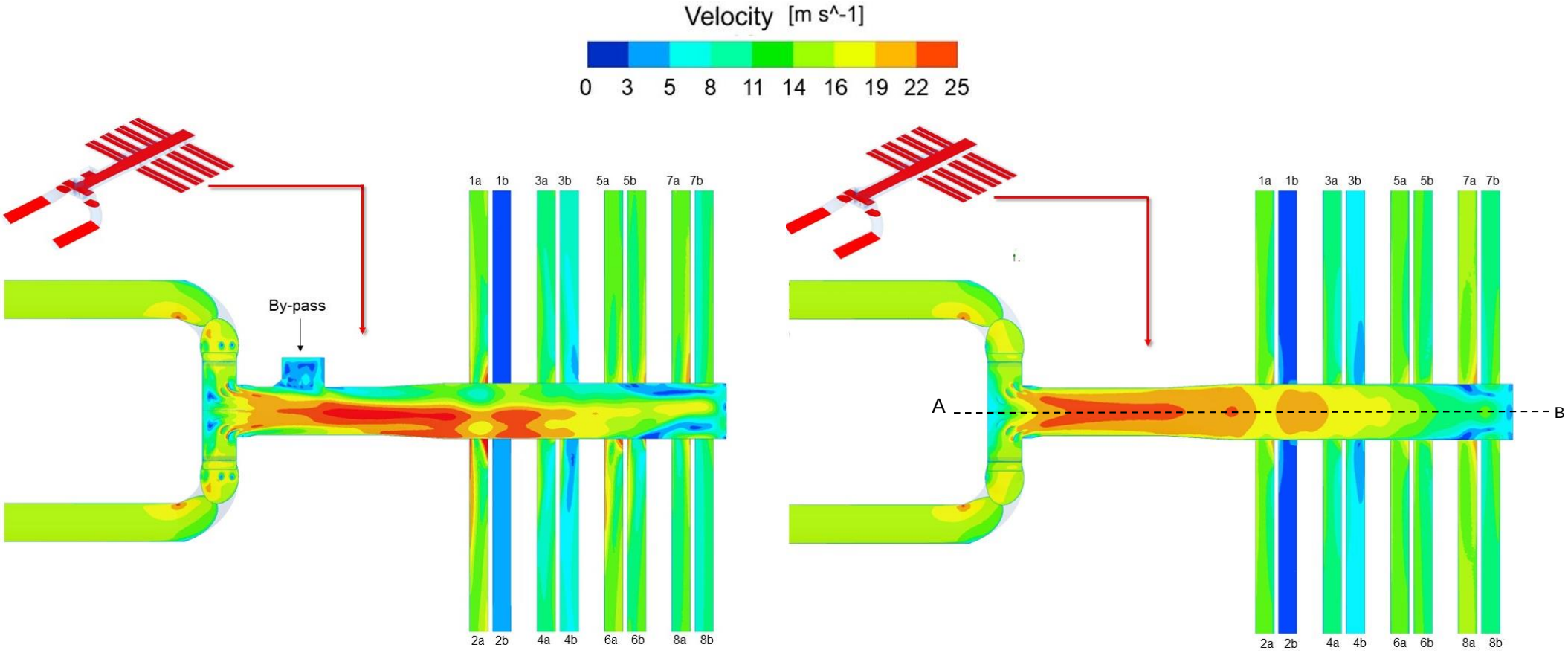

Figure 14, shows the velocity field plotted in vertical planes at the straight segment and demonstrates more clearly the flow separation from the wall in the bypass's side causing the velocity increase in the opposite side.

Figure 14: Velocity field plotted in the vertical planes at the straight segment.

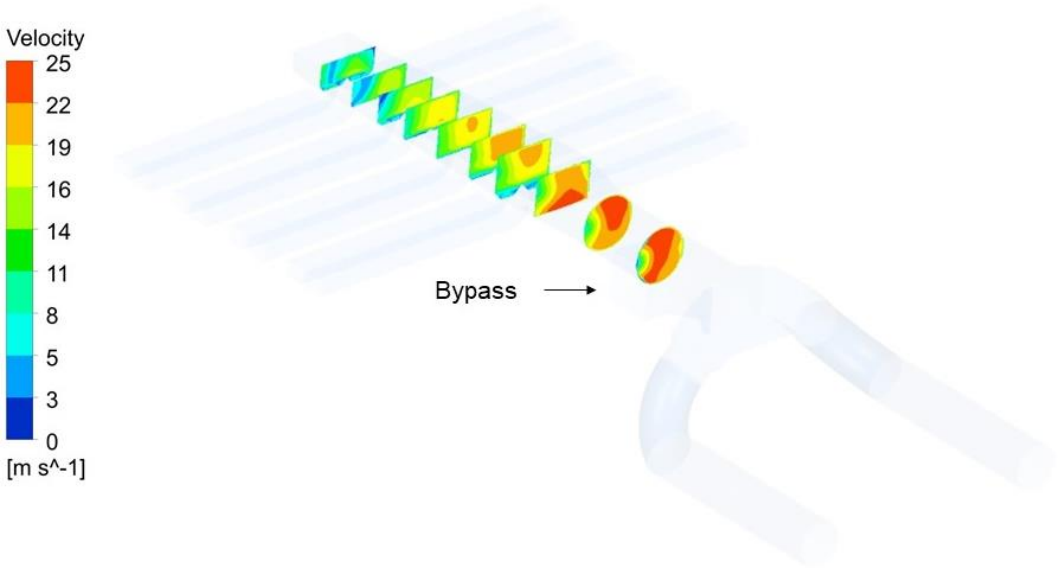

Figure 15 presents the velocity field in the duct outlets for more details about the duct outlets velocity distribution in the existing design scenario.

Curves are regions where there is greater friction of the flow with the duct walls and, as mentioned earlier, they need more attention in terms of maintenance. Figure 15 shows high velocities (above 22 m/s) in the curves upstream of exits 1a, 2a, 4a, 4b, 6a, and 6b. This result corroborates with Figure 14, which shows the velocity increase at outlets 2, 4 and 6 due to the effect generated by the bypass presence. Such outlets also have higher velocity gradients, varying between 8 and 25 m/s, contributing to the pressure drop increase in these regions and requiring more energy expenditure.

Outlets 1b and 2b stand out for their lower velocity values and velocity gradient (below 8 m/s) compared to the other outlets, which has been discussed in Figures 10, 12 and 13. Thus, another analysis in the outlets velocity is presented in Figures 16 and 17, which shows the vertical plane velocity vectors at outlets 2 and 4, and at outlets 5 and 7 for the two scenarios, respectively.

Figure 15: Velocity field plotted at outlets 2 and 4 for the existing design scenario (a).

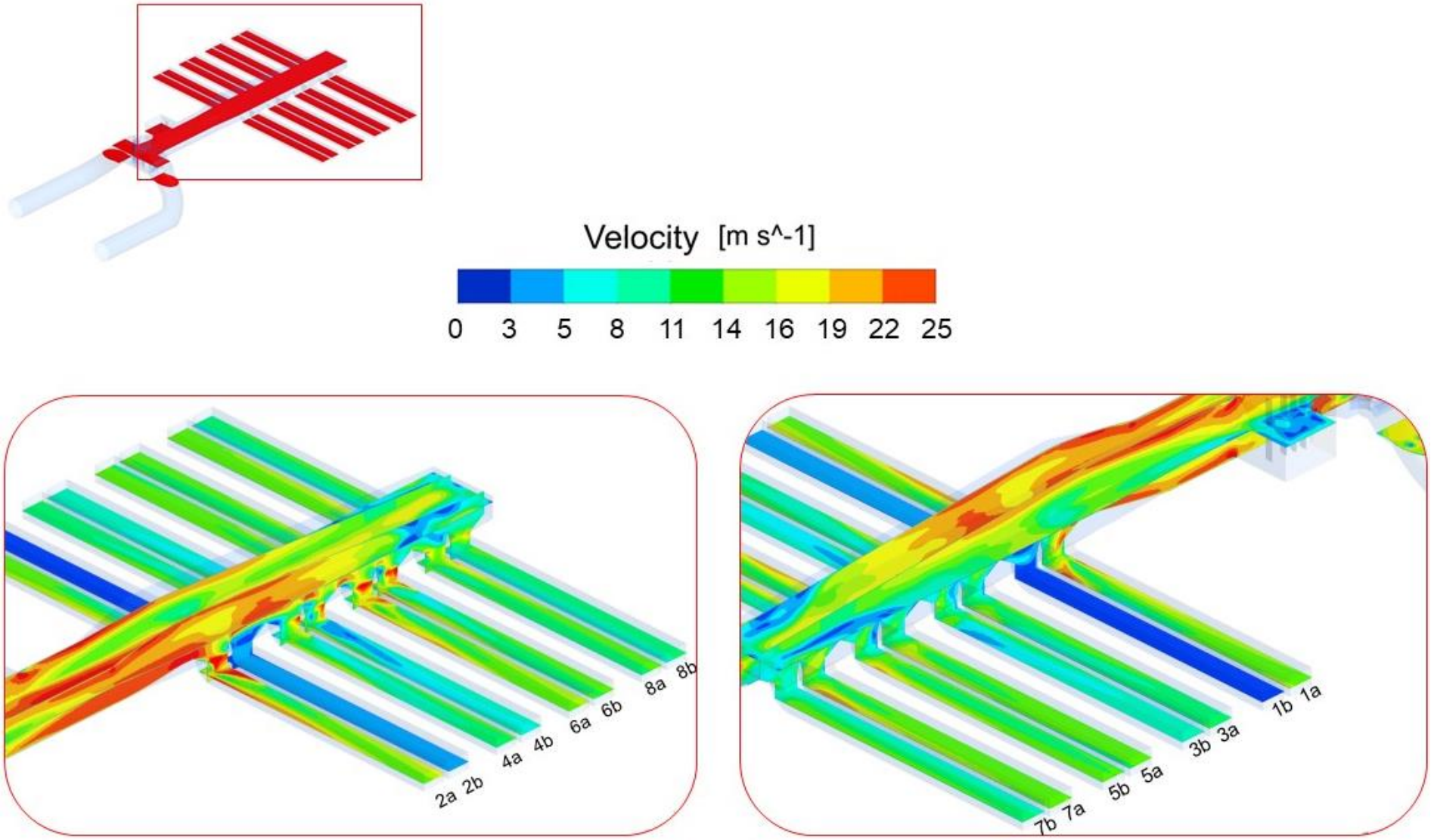

Figure 16 shows that in both scenarios, the main flow, that was in the direction of the straight segment, when encounters the first outlet (2a) accelerates towards it. The air flow seems to be more intended to outlet 2a given that it is a low-pressure region. Consequently, as outlet 2b is close from outlet 2a, the amount of flow that should intend to it is decelerating and recirculating (where the pressure gradient is smaller compared to the first outlet). Therefore, the result shows that this is a problem in the outlets design configuration and that the presence of the bypass is not the main reason why the flow distribution is so different in outlet 2b from outlet 2a. The same results were found for the other side of the duct, which means that outlets 1a and 1b had the same flow pattern as outlets 2a and 2b.

Nevertheless, Figure 17a shows that the recirculation region observed in Figure 10 is a vortex between outlets 5b and 7a. It is possible to visualize that the main flow at low velocity (below 8 m/s) combines with the flow reflected by the wall coming from the opposite direction, forming this big vortex susceptible to particle settling. As the air velocity in the other side of the straight segment is higher (see Figure 14), no vortex was found in this side. Additionally, it can be inferred that this recirculation area in Figure 17a was generated due to the flow pattern variation generated by the bypass presence since this vortex is not generated in Figure 17b, which illustrates the same outlets presented in Figure 17a for the hypothetical scenario without the bypass.

Typically, the average inlet velocity for fabric filters are designed in a range from 3 to 5 m/s (verbal information)[2]. If the inlet velocity is higher than this range, as can be seen in Figure 16 and 17, there is a potential velocity increase in some fabric regions, enhancing the air to cloth ratio in these areas. As a negative consequence, the filtration efficiency can be affected and the bags life span can reduce.

[2] Rafael Sartim gave information in May 2020.

Figure 16: Vertical plane velocity vectors located at outlets 2 and 4 for the existing design (a) and the hypothetical duct without the bypass (b).

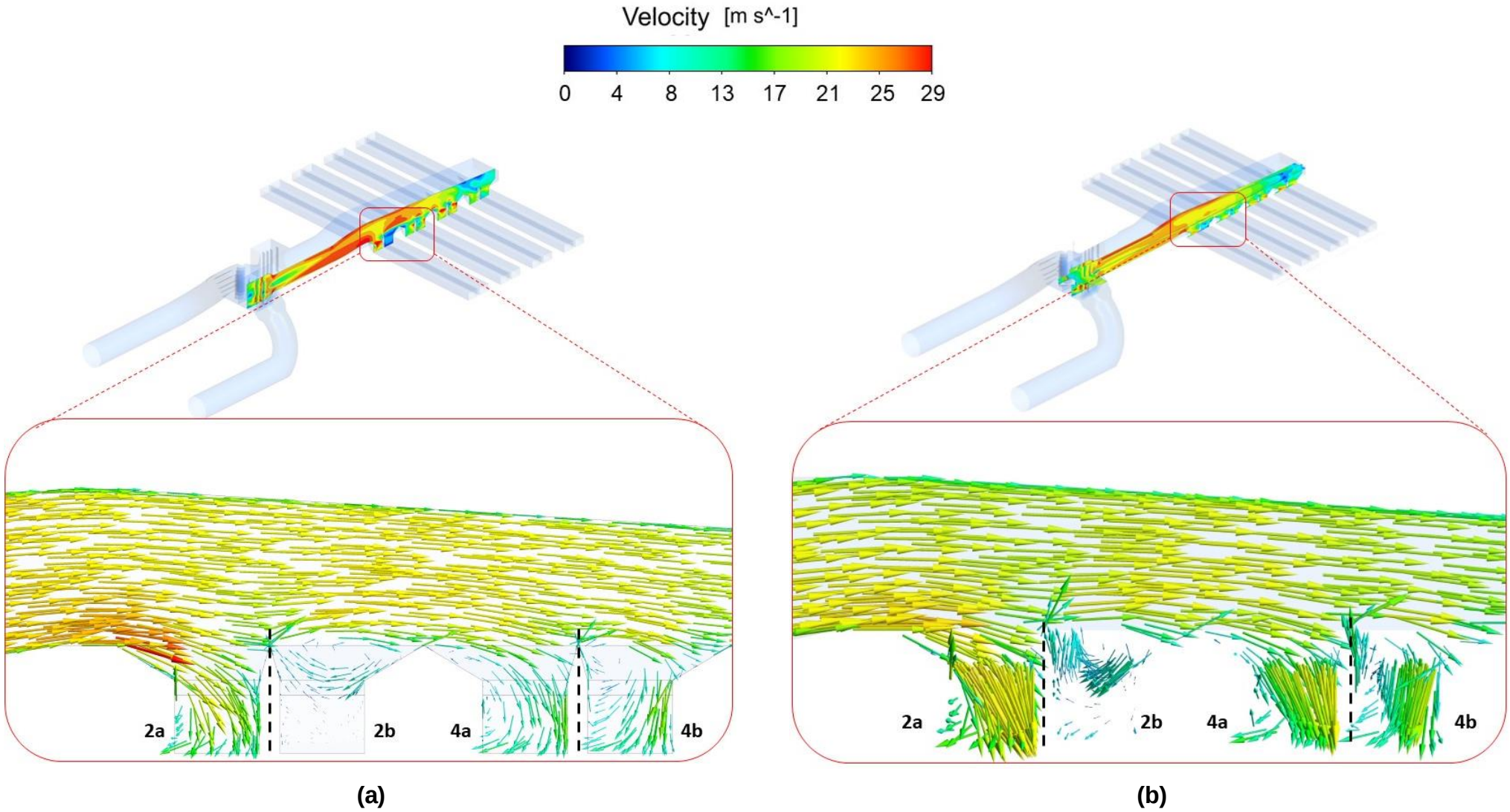

(a) **(b)**

Figure 17: Vertical plane velocity vectors located at outlets 5 and 7 for the existing design (a) and the hypothetical duct without the bypass (b).

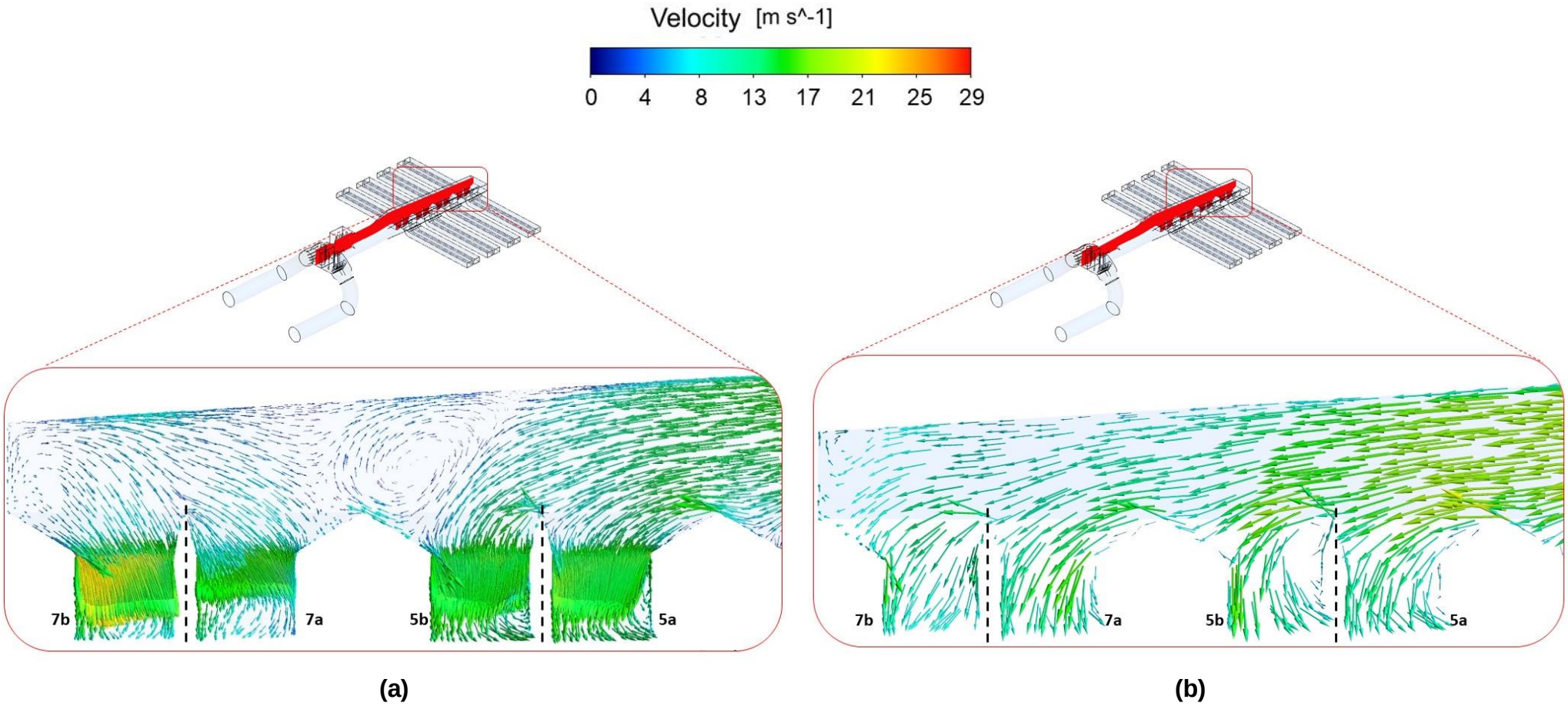

(a) **(b)**

The total static pressure variation calculated through the simulation results for the existing design scenario was 329.53 Pa, while for the hypothetical scenario without the bypass the value was equal to 173.32 Pa, representing a decrease of 52.60%.

Figure 18 shows the pressure field for the existing duct scenario (a) and the hypothetical scenario without the bypass (b). As can be seen in the first scenario, there is a higher pressure gradient from the duct entrance to the bypass, showing a variation of -278,87 Pa in the zoom given in the bypass region. It is also important to note that the bypass presence caused a whole variation in the air flow pattern in the straight segment and in the duct outlets, which is also responsible for causing greater pressure variations.

Moreover, in the first outlet (2b) the pressure varies from -200 Pa to 450 Pa, while in outlet 2b there is no such difference in the pressure gradient (from -70 to -5 Pa). Therefore, this result corroborates with the discussions in Figure 16, on which was seen a higher air flow in the outlet 2a direction than in the outlet 2b direction.

In this way, it is possible to notice a smaller pressure variation in the hypothetical scenario without the bypass (b). This case showed a pressure gradient equal to -138.11 Pa in the zoom given in region that the bypass is located in the existing scenario (a). Thus, the bypass can be considered an important influence to the total static pressure distribution in the duct work.

Figure 18: Pressure distribution in the existing design scenario (a) and in the hypothetical scenario without the bypass (b).

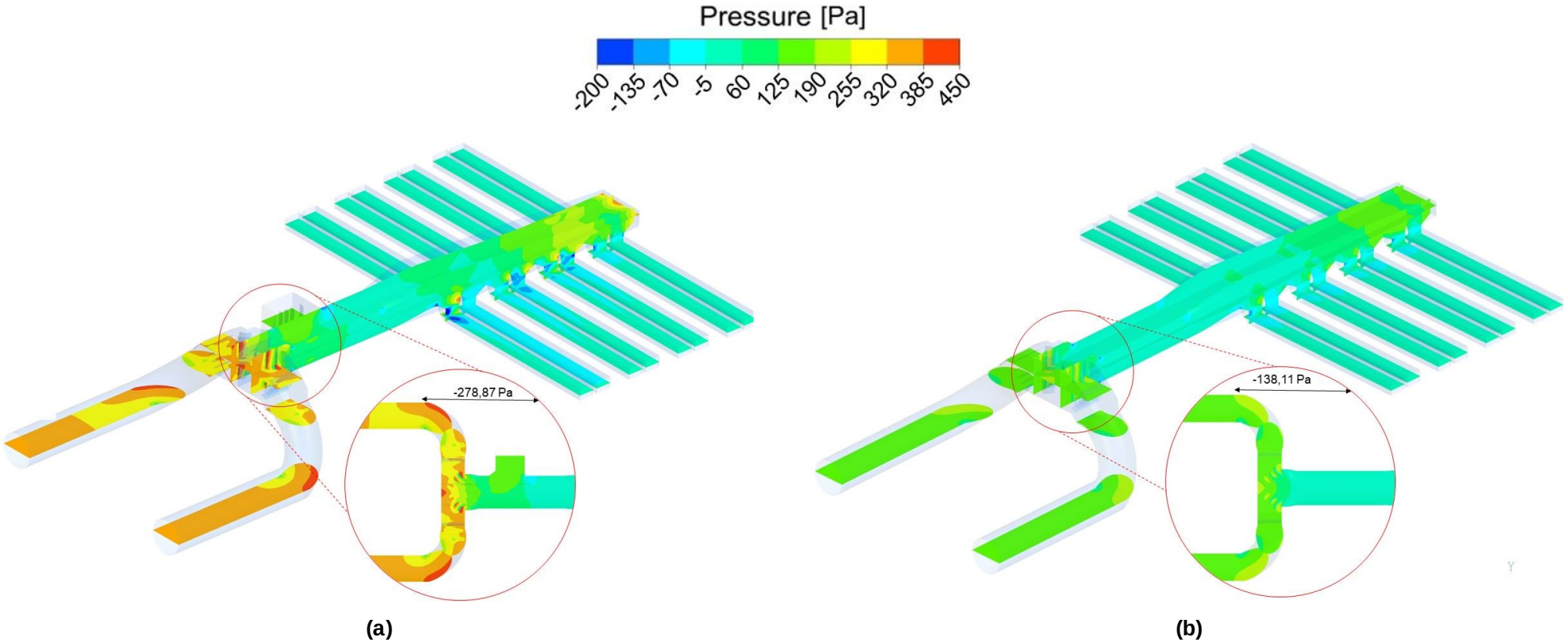

(a) **(b)**

5.2 PARTICLE DISTRIBUTION

Due to the air recirculation in regions with vortexes, hydrated lime particles get trapped and can settle. The particle disperses less in low-velocity air zones than in high-velocity zones, therefore, lime deposition is generated in low-velocity areas.

As mentioned in section 4.2.1, there are some circular plates in the existing duct located in the straight segment that were not considered in the simulation. Thus, it is recommended to simulate them to evaluate their position and influence on hydrated lime dispersion.

Figure 19 shows the hydrated lime particle trajectory for the two scenarios. In the zoom in Figure 19a is possible to see more clearly the hydrated lime injections and the guide vanes distributing the particle flow to the main duct.

In the first scenario (a), a particle settling region is observed in the same highlighted areas in Figure 10 (bypass and between outlets 5b and 72). The region at the end of the duct represents a vortex that was influenced by the reflection of the main stream in the wall presented in Figure 17a.

In the same way that outlets 1b and 2b stood out in the air flow analysis, now they are in this discussion since they seem to have no particle trajectory. This is an important point of the work, as it shows how the air flow really influences hydrated lime particles transport.

The second scenario (b) also indicates a particle settling region at the end of the duct due to the wall reflection. The hydrated lime distribution is more homogeneous in outlets 3, 4, 5, 6, 7, and 8. However, outlets 1 and 2 seems to have few particle trajectories, and they also have less fluid streamlines in this scenario (see Figure 11).

The minimum recommended velocity for low-density particles in industrial ventilation ducts is 10 m/s (ACGIH, 2019a) in order to prevent from particle settling. As seen in Figure 19, the particle velocity is below the recommendation in many sections of the duct, which can lead to risk of particle deposition.

Figure 19: Hydrated lime particles trajectory for the existing design scenario (a) and the hypothetical scenario without the bypass (b).

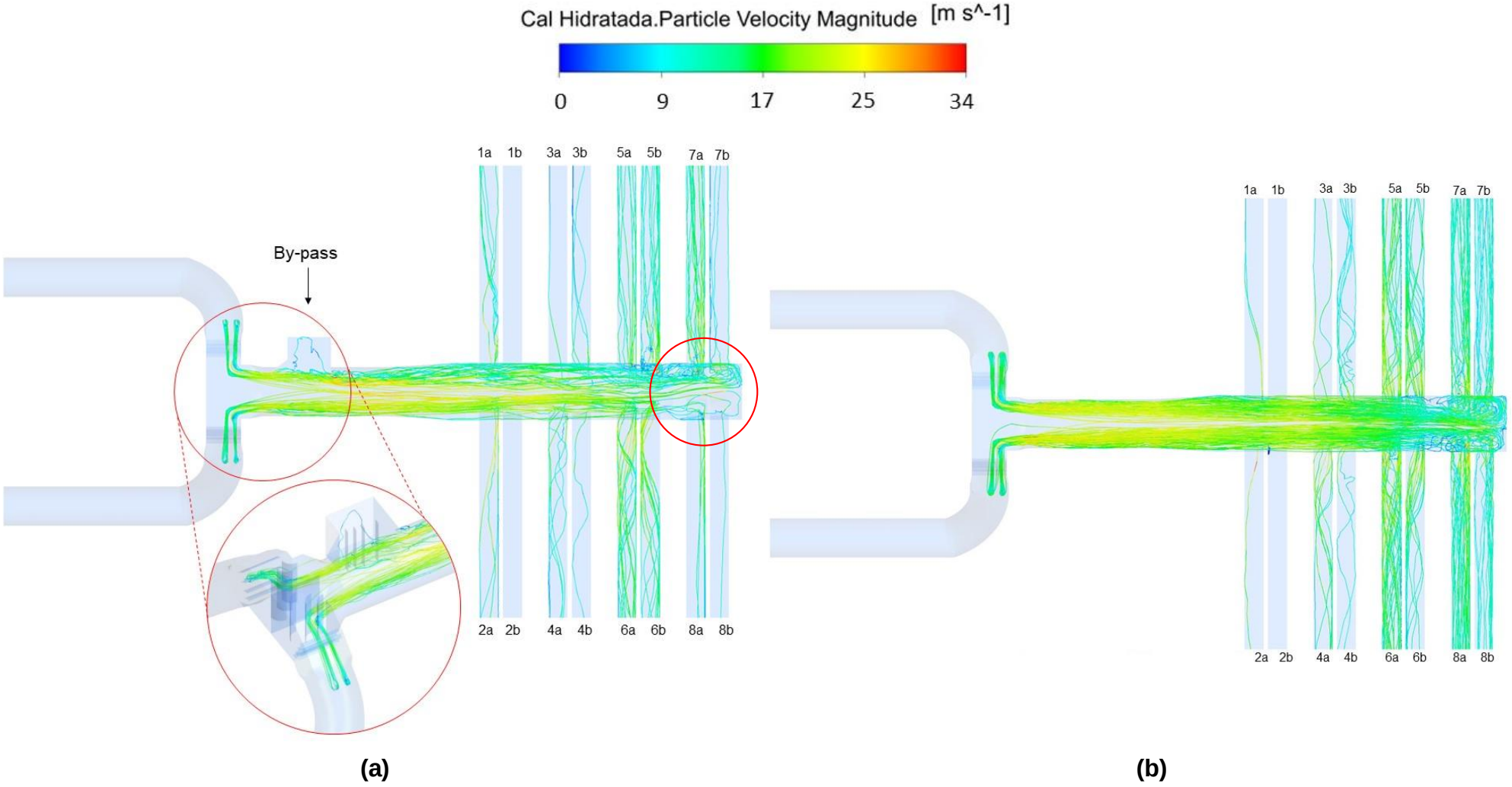

Figure 20 presents the hydrated lime mass flow distribution at the fabric filter compartments inlet that correspond to the duct outlets for the two scenarios. It is worth to remember that this material is used for the fabric bags precoating, and influences the filtration performance. Therefore, it is essential that the hydrated lime mass flow distribution is homogeneous in the compartments inlet so the material can cover all the bags evenly.

However, as shown in Figure 20, the hydrated lime mass flow distribution is heterogeneous in both scenarios. The total mass flow result in the system outlet was also similar for both scenarios. While 0.167 kg/s of hydrated lime was injected in the system, the mass flow sum in the outlets was 0.166 kg/s for the existing geometry; and 0.165 kg/s for the geometry without the bypass. This result indicates that the rest (0.5% and 1%, respectively) got trapped, that is, settled in the duct.

The compartments 1 and 2 show hydrated lime mass flow near zero. These compartments contemplate outlets 1b and 2b where less particle trajectories were found in Figure 19. As the air flow is responsible for transporting the hydrated lime particles, as a consequence of the low air velocity in 1b and 2b outlets, the mass flow inside them was also low. Despite the deposited mass flow in the duct is not significant, the result suggested that the hydrated lime is not fulfilling its purpose of precoating all the fabric bags, since the fluid and particle distribution in the filter compartments is not uniform, increasing the necessity for design improvements in the duct outlets geometry.

It is worth remembering that this work did not considered the chemical reactions between the hydrated lime particles and the sulfur present in the gas. Such a reaction can contribute to the hydrated lime content reduction, which is a perspective for future works analysis.

Figure 20: Average mass flow at the fabric filter compartments inlet for the existing design scenario (a) and the hypothetical scenario without the bypass (b).

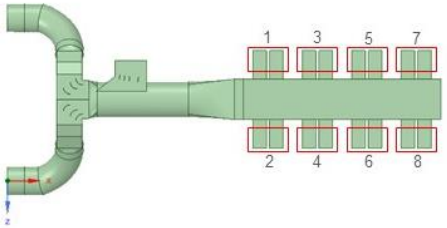

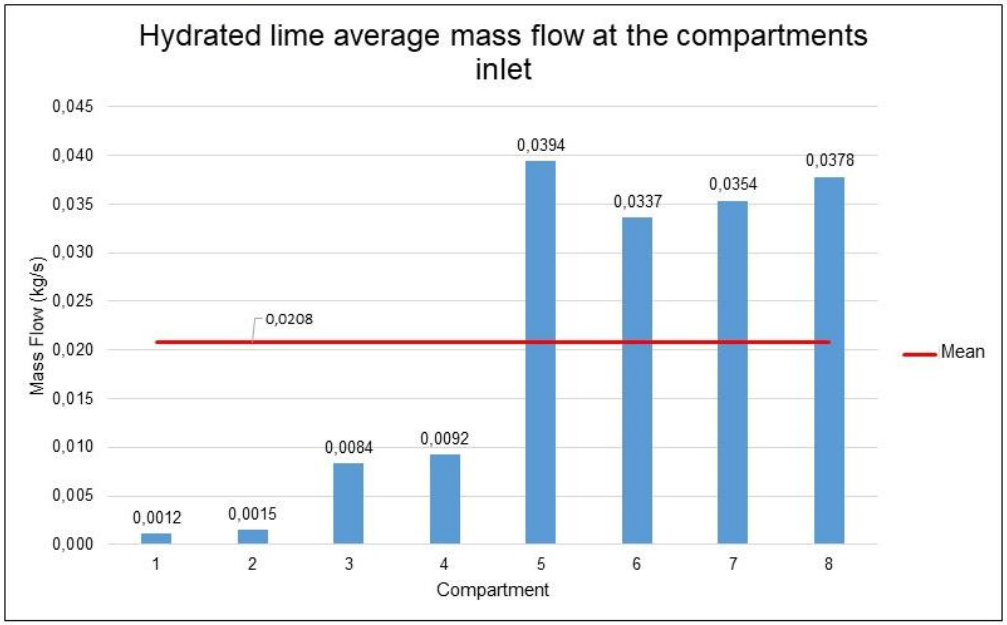

(a)

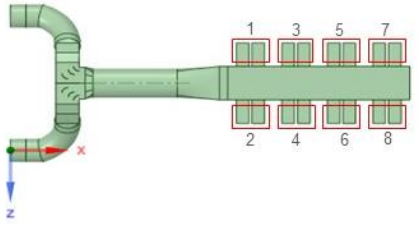

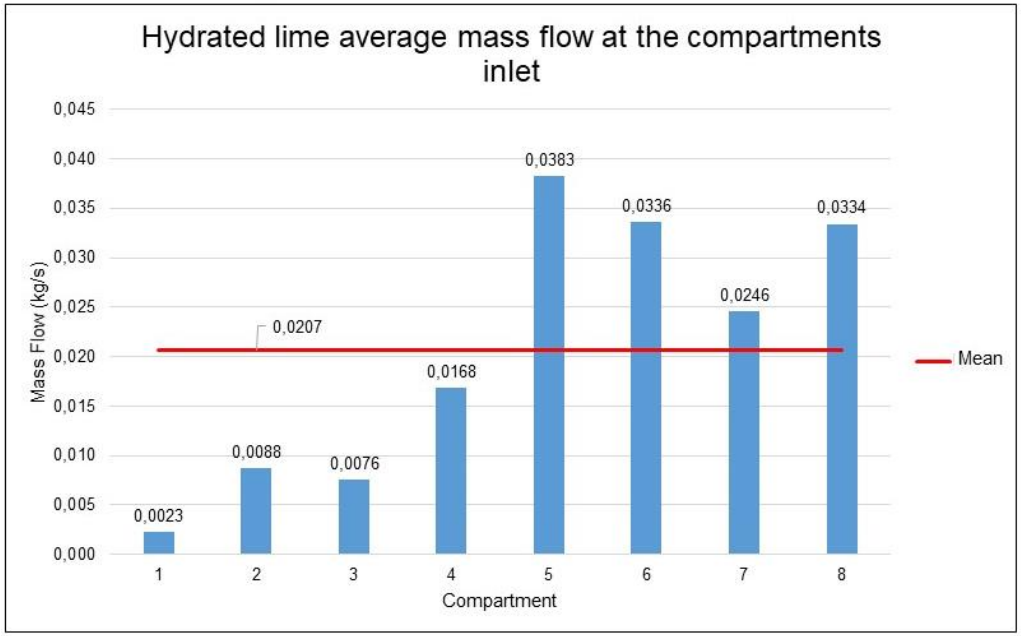

(b)

Particle residence time is the amount of time a particle spent in the domain (ANSYS, 2017). It is an important variable that also gives an idea about particle deposition areas, which means that regions with higher values of residence time are more suggestive for particle settling.

As shown in Figure 21, the residence time distribution in the computational domain is plotted for the two cases. The differences in the mean residence time indicate that the complex velocity field strongly influences the particles path. In the existing geometry scenario (a) and in the hypothetical scenario without the bypass (b), the average particle residence time is around 3 seconds at the straight segment, indicating low probability of particle settling in this region. But, in the end of the duct, the particle residence time was higher (around 6 seconds), which is an area with vortexes with low velocity, suggesting higher particle settling probability.

The maximum particle residence time in both scenarios was 11 seconds in outlet 5b for scenario (a); and in outlets 2b, 5b, 7b, and 8b for scenario (b). In the firsts outlets (1, 2, 3, and 4), for both scenarios, the particle residence time was lower (around 3 seconds) than in the lasts ones. This is another important result because outlets 1, 2, 3, and 4 have less hydrated lime mass flow than outlets 5, 6, 7, and 8 (see Figure 20). Thus, the average particle residence time histogram at the fabric filter compartments inlet that correspond to the duct outlets for the two simulated scenarios is plotted in Figure 21.

Figure 21: Particle residence time track lines for the existing design scenario (a) and the hypothetical scenario without the bypass (b).

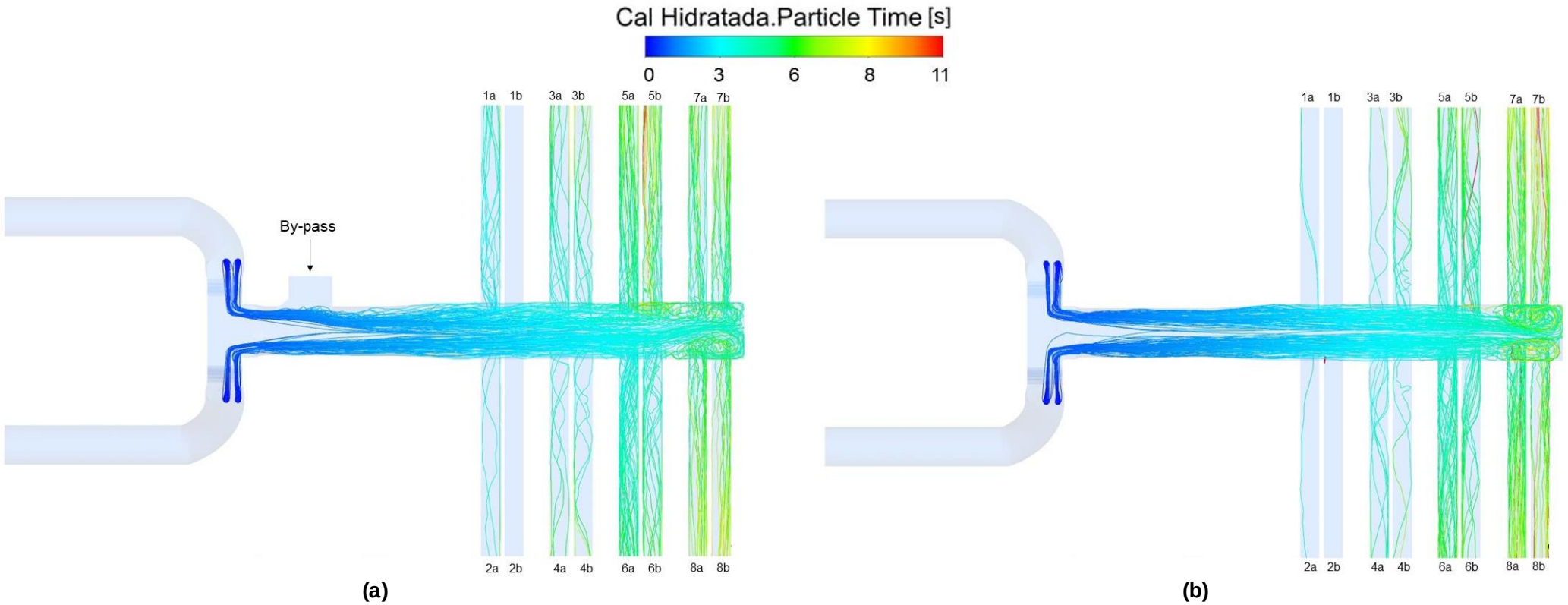

The particle residence time histogram for both scenarios was similar. In the two cases the average residence time was 6 seconds, differently from Figure 21 that showed an average residence time in the order of 3 seconds.

It is possible to visualize that this variable was not evenly distributed between the filter compartments. Compartments 1 and 2 had the lowest average residence time values, that also had the lowest values for hydrated lime mass flow (see Figure 20). It can be seen that residence time is not directly proportional to mass flow, and is more influenced by the flow pattern, which is highly affected by the duct geometry. Although these firsts compartments are less favorable to carry particles due to the low velocity airflow (see Figure 11 and 12), the transported particles into these compartments arrive more quickly, not necessarily because they have higher velocity.

The maximum average residence time in the existing design scenario (a) was 7,1 seconds in compartment 8 (which was the same with higher average air velocity), and in the hypothetical scenario without the bypass was 6,9 seconds in compartments 4 and 7. Additionally, in both scenarios the standard deviation was also similar: 0,85 for scenario (a), and 0,89 for scenario (b).

Figure 22: Particles residence time histogram at the fabric filer compartments inlet for the current scenario (a) and the scenario without the bypass (b).

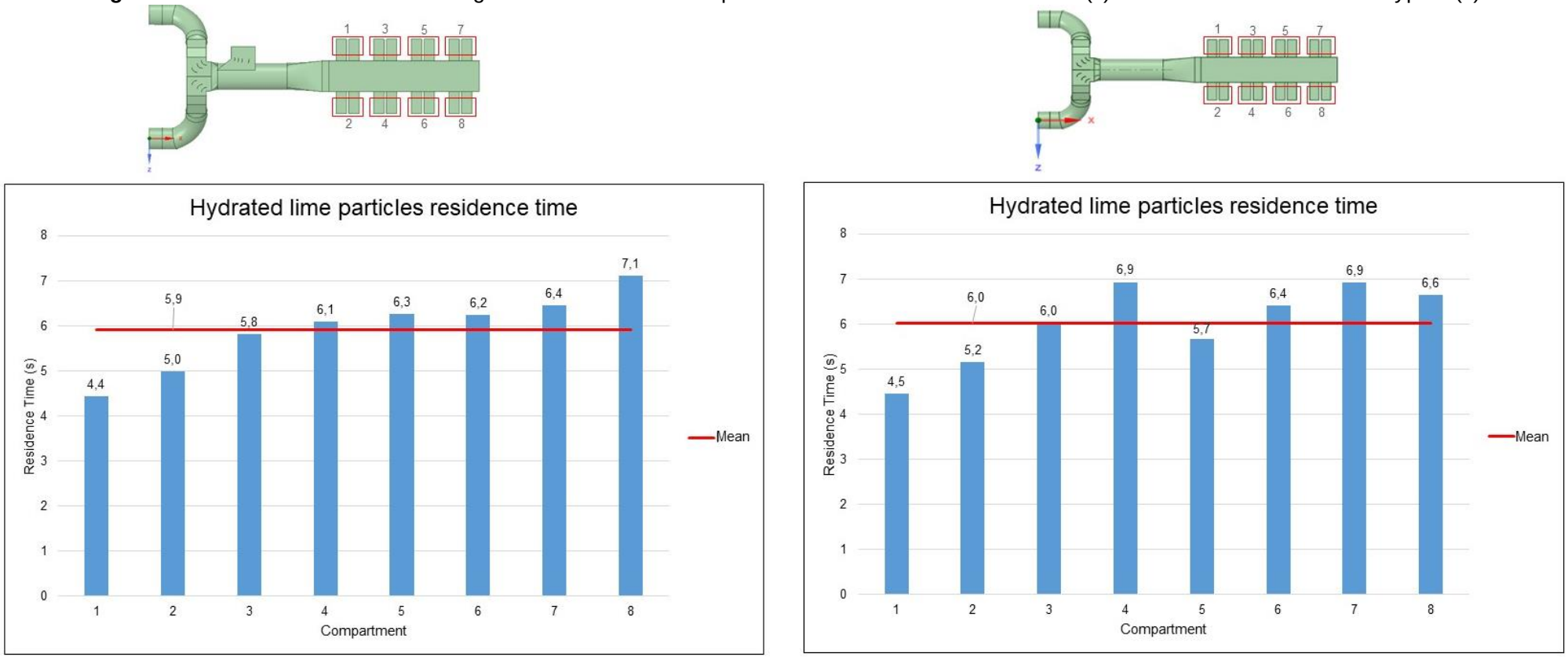

(a) **(b)**

6 CONCLUSIONS

The present work carried a CFD simulation of a two-phase gas-solid flow in a fabric filter inlet duct, which is based in an industrial case part of a sinter plant Primary Dedusting System. The simulations were perfomed using real data from the dedusting process with the commercial software Ansys Fluent. The study aimed to analyze the fluid characteristics and hydrated lime particles distribution, used to precoate the filtering bas and enhance the filtration efficiency. Consequently, the duct geometry influence on the biphasic flow inside the fabric filter inlet duct and, therefore, on the equipment performance was evaluated.

The simulation analysis showed a heterogeneous velocity field inside the duct caused by the bypass presence that generated the flow separation from the wall, enhancing the air velocity in the opposite side and changing the flow pattern in the outlets. Subsequently, the air flow at the bypass's side decelerated forming a vortex with low velocity between outlets 5b and 7a. This phenomenon was confirmed after comparing the existing duct scenario with a hypothetical scenario without the bypass, which showed a homogeneous airflow distribution and no vortex in this region. This area stood out because it has a potential for particles settling. The velocity field at the duct outlets was also heterogeneously distributed. Outlets 1b and 2b were highlighted since they had lower air flow velocity and less streamlines than the others. However, this same result was found in the hypothetical scenario without the bypass, suggesting that another characteristic in the duct outlets configuration influenced this result. As a consequence of this change in the flow pattern, the static pressure was another variable highly affected in the simulations. While the total pressure drop in the existing duct scenario was 329.53 Pa, in the hypothetical scenario without the bypass the value was equal to 173.32 Pa, representing a decrease of 52.60%. Besides, the results for the static pressure distribution showed a greater pressure gradient at outlet 1a and 2a, which possibly caused the air flow to be more accentuated for these outlets than for outlets 1b and 2b.

The continuous injections of 0.167 kg/s of hydrated lime in the studied duct were analyzed and the results demonstrated that the particle's amount trapped in the duct was insignificant, since the total mass flow trapped in the duct was 0.5% in the first scenario and 1% in the second scenario. However, as the particle distribution is

highly influenced by the air flow pattern, the hydrated lime mass flow in the filter compartments was also heterogeneous. For instance, the compartments 1 and 2 had the lowest hydrated lime mass flow, which contemplate the outlets 1b and 2b. Therefore, this result indicates that the alkaline material is not covering all the compartments equally in order to precoate the filtration bags.

Thus, it is possible to conclude that the fabric filter performance is directly affected by such not uniform air and hydrated lime distribution in its inlet duct. Some compartments may be operating outside the range of the inlet air velocity recommended by ACGIH (2019a) to obtain an adequate filtration velocity in the bags. In addition, the compartments are not receiving equal amounts of hydrated lime, so the precoating is probably not occurring on all bags. Given the simulation presented in this work, the results indicate the importance of analysis in fabric filters that has a bypass designed, due to its potential in changing the gas-solid flow pattern. The CFD tool proved to be powerful for this type of analysis in existing equipment and projects in conception.

7 RECOMENDATIONS FOR FUTURE WORKS

Since this work did not consider the circular plates presence located in the straight segment (see section 4.2.1), it is important to carry out future simulations with these devices to assess what should be the most appropriate position in order to provide a better hydrated lime particles spread, and to have a homogeneous particle distribution in the fabric filter entrance.

Another study for the future will be a simulation of the gas and hydrated lime chemical reactions to evaluate the desulfurization process inside the duct. Such a study can simulate distinct cases changing the hydrated lime inlet mass flow and duct configuration in order to obtain the most optimized scenario.

As the focus of this simulation was the inlet duct equipment, further work could be developed on the entire filter.

REFERERENCES

ACGIH - American Conference of Governmental Industrial Hygienists. Industrial Ventilation: A Manual of Recommended Practice for Design. 30th edition, 2019a.

ACGIH - American Conference of Governmental Industrial Hygienists. Industrial Ventilation: A Manual of Recommended Practice for Operation and Maintenance. 1rst edition, 2019b.

ADAM, N.; EVERITT, P.; RIFFAT, S. B. Aerosol deposition in ventilation ducts. **International Journal of Energy Research**, v. 20, n. 12, p. 1095–1101, 1996.

ANDRADE, Bárbara K.S.A.; SARTIM, Rafael; AGUIAR, Monica L. Efficiency of Collection of Particulate Matter and Maximum Pressure Drop of Precoating. **Filtech**, 2019.

ANDRADE, Bárbara K.S.A. **Avaliação do precoating e dos meios filtrantes para filro de mangas do processo de despoeiramento secundário da aciaria.**São Carlos: [s.n], 2019.

ANDREÃO, Willian L.; ALBUQUERQUE, Taciana T.A.; KUMAR, Prashant. Excess deaths associated with fine particulate matter in Brazilian cities. Atmospheric Environment, v. 194, n. May, p. 71–81, 2018. Disponível em: <https://doi.org/10.1016/j.atmosenv.2018.09.034>.

ANSYS, A. F. 18.2 Theory Guide *ANSYS inc,* 2017.

BARNETT, Tim. Improving the performance of fabric filter dry dust collection equipment. Filtration & separation, v. 37, n. 2, p. 28-32, 2000.

BERNABÉ, Ana Clara Alves. Avalização do escoamento e proposição de melhorias em um filtro de magas utilizando fluidodinâmica computacional (CFD). . Vitória: [s.n.], 2016.

BRASIL. RESOLUÇÃO CONAMA nº 5, de 15 de junho de 1989. **Dispõe sobre o Programa Nacional de Controle da Poluição do Ar – PRONAR**. 1989. Brasília: DOU, 25 de agosto de 1989, pág. 14713 – 14714.

BRASIL. Resolução nº 382, de 26 de dezembro de 2006. **Estabelece os limites máximos de emissão de poluentes atmosféricos para fontes fixas.** Brasília: Dou, 2 jan. 2007. Seção 1, p. 131-137.

BRASIL. Resolução nº 436, de 22 de dezembro de 2011. **Estabelece os limites máximos de emissão de poluentes atmosféricos para fontes fixas instaladas ou com pedido de licença de instalação anteriores a 02 de janeiro de 2007.**. Brasília: Dou, 26 dez. 2011. Seção 1, p. 304-311.

BRASIL. Resolução nº 491, de 19 de novembro de 2018. **Dispõe sobre padrões de qualidade do ar.** Brasília: DOU, 21 nov. 2018. Seção 1, p.155.

CABLE, Matt. An Evaluation of Turbulence Models for the Numerical Study of Forced and Natural Convective Flow in Atria by A thesis submitted to the Department of Mechanical and Materials. n. May, 2009.

CHANG, Ping et al. Minimizing DPM pollution in an underground mine by optimizing auxiliary ventilation systems using CFD. Tunnelling and Underground Space Technology, v. 87, n. January, p. 112–121, 2019. Disponível em: <https://doi.org/10.1016/j.tust.2019.02.014>.

COOPER, C. D.; ALLEY, F. Air Pollution Control: A Design Approach. 3rd. ed. [S.l.]: Waveland Press, 2002.

DAI, Qi Li et al. Characterization and source identification of heavy metals in ambient PM10 and PM2.5 in an integrated Iron and Steel industry zone compared with a background site. Aerosol and Air Quality Research, v. 15, n. 3, p. 875–887, 2015.

DAMIAN, Ricardo Barbosa et al. Improving the performance of asphalt plant components using CFD. n. 1997, p. 10, 2004.

DE ALMEIDA SANTOS, Bruno Orlando et al. Numerical modeling of flow into primary dedusting system of a 130t converter. Journal of Materials Research and Technology, v. 1, n. 1, p. 21–26, 2012. Disponível em: <http://dx.doi.org/10.1016/S2238-7854(12)70005-4>.

DULLIEN, Francis AL. **Introduction to industrial gas cleaning**. San Diego: Academic Press, 1989.

ELSAYED KHAIRY, K.; LACOR, Chris. Optimization of the cyclone separator geometry for minimum pressure drop using mathematical models and CFD simulations. Chemical Engineering Science, v. 65, n. 22, p. 6048–6058, 2010. Disponível em: <http://dx.doi.org/10.1016/j.ces.2010.08.042>.

FOX, Robert W.; MCDONALD, Alan T.; PRITCHARD, Philip J. Introdução à mecânica dos fluidos. 8. ed. [S.l.]: LTC, 2014.

GANEGAMA BOGODAGE, Sakura; LEUNG, Andrew Y.T. CFD simulation of cyclone separators to reduce air pollution. Powder Technology, v. 286, p. 488–506, 2015. Disponível em: <http://dx.doi.org/10.1016/j.powtec.2015.08.023>.

GUTIÉRREZ ORTIZ, F. J.; OLLERO, P. A realistic approach to modeling an in-duct desulfurization process based on an experimental pilot plant study. Chemical Engineering Journal, v. 141, n. 1–3, p. 141–150, 2008.

HASANBEIGI, Ali; KHANNA, Nina; PRICE, Lynn. Air Pollutant Emissions Projections for the Cement and Steel Industry in China and the Impact of Emissions Control Technologies. . [S.l: s.n.], 2017.

KIM, Ki Hyun; KABIR, Ehsanul; KABIR, Shamin. A review on the human health impact of airborne particulate matter. Environment International, v. 74, p. 136–143, 2015. Disponível em: <http://dx.doi.org/10.1016/j.envint.2014.10.005>.

LAUNDER, Brian. Progress in the development of a Reynolds-stress turbulence closure. n. October, p. 30, 1974.

LI, Xiaolin et al. Atmospheric lead pollution in fine particulate matter in Shanghai, China. Journal of Environmental Sciences, v. 21, n. 8, p. 1118–1124, 2009. Disponível em: <http://dx.doi.org/10.1016/S1001-0742(08)62390-6>.

LIMA, Wagner Ferreira. Análise da distribuição de ar em um filtro de mangas utilizando dinâmica dos fluidos computacional. . Belo Horizonte: [s.n.], 2019.

LU, Hao; WANG, Yuanhao. Particle deposition in ventilation ducts: A review. Building Simulation, v. 12, n. 5, p. 723–734, 2019.

MALISKA, Clovis R.. **Transferência de Calor e Mecânica dos Fluidos Computacional.** 2. ed. Rio de Janeiro: LTC, 2004. 453 p.

MAROCCO, Luca; MORA, Alessandro. CFD modeling of the Dry-Sorbent-Injection process for flue gas desulfurization using hydrated lime. Separation and Purification Technology, v. 108, p. 205–214, 2013. Disponível em: <http://dx.doi.org/10.1016/j.seppur.2013.02.012>.

MORSI, S. A.; ALEXANDER, A. J. An investigation of particle trajectories in two-phase flow systems. Journal of Fluid Mechanics, v. 55, n. 2, p. 193–208, 1972.

NIELSEN, Niels Finderup et al. Fabric Filter Optimization using Computational Fluid Dynamics Abstract : 2011, Australia, Australian Capital Territory, Canberra: [s.n.], 2011. p. 239–243. Disponível em: <https://pdfs.semanticscholar.org/f053/59a11505998f189bc8718ea84741f7614329.pdf>.

NOROUZI, Hamid Reza et al. **Coupled CFD-DEM modeling: formulation, implementation and application to multiphase flows**. John Wiley & Sons, 2016.

OLIVEIRA, Louise Schmitd. Simulação em CFD do escoamento no interior de um ciclo-filtro industrial Simulação em CFD do escoamento no interior de um ciclo-filtro industrial Vitória. . Vitória: [s.n.], 2018.

PATANKAR, S. V.; SPALDING, D. B. Numerical prediction of three-dimensional flows. 1972.

PARK, Sangcheol et al. Non-uniform filtration velocity of process gas passing through a long bag filter. Journal of Hazardous Materials, v. 365, n. November 2018, p. 440–447, 2019. Disponível em: <https://doi.org/10.1016/j.jhazmat.2018.10.098>.

PEREIRA, Thomas Wilis Cândido et al. The influence of the fabric filter layout of in a flow mass filtrate. Journal of Cleaner Production, v. 111, p. 117–124, 2016.

RAVERT, Ed. Precoating new filters for better airflow, longer filter life. Powder and Bulk Engineering, v. 20, n. 10, 2006.

REMUS, Rainer et al. Best Available Techniques (BAT) Reference Document for Iron and Steel Production. [S.l: s.n.], 2013. v. BREF-IS. Disponível em: <http://eippcb.jrc.ec.europa.eu/reference/BREF/IS_Adopted_03_2012.pdf>.

RIZZO, E. M. S. *Introdução aos Processos Siderúrgicos*, São Paulo, ABM, 2005.

ROCHA, Sandra Mara S. et al. Applications of CFD techniques in the design of fabric filters. Chemical Engineering Transactions, v. 39, n. Special Issue, p. 1369–1374, 2014.

SCHILLER, Sascha; HELLMICH, Christoph; SCHMID, Hans Joachim. Evaluation of the Efficiency of Filtration Processes Using Precoat Materials. Chemical Engineering and Technology, v. 39, n. 3, p. 491–498, 2016.

SCHMIDT, E.; LÖFFLER, F. Preparation of dust cakes for microscopic examination. Powder Technology, v. 60, n. 2, p. 173–177, 1990.

SCHNELLE, Karl B.; BROWN, Charles A. Air pollution control technology handbook. [S.l: s.n.], 2002.

SHI, Guoqing et al. Unsteady simulation for optimal arrangement of dedusting airduct in coal mine heading face. **Journal of Loss Prevention in the Process Industries**, v. 46, p. 45-53, 2017.

SHIH, T. H et al. A New k-e Eddy Viscosity Model for High. p. 34, 1994.

SILVA, Ricardo Galdino da. **Estudo numérico de movimentação de partículas em escoamentos**. 2006. Dissertação (Mestrado em Engenharia Mecânica) - Escola Politécnica, Universidade de São Paulo, São Paulo, 2006. doi:10.11606/D.3.2006.tde-08032007-181139. Acesso em: 2019-11-13.

SONG, Jianfei et al. Experimental and CFD study of particle deposition on the outer surface of vortex finder of a cyclone separator. Chemical Engineering Journal, v. 309, p. 249–262, 2017. Disponível em: <http://dx.doi.org/10.1016/j.cej.2016.10.019>.

TANG, Qiang et al. Numerical simulation of flue gas desulfurization characteristics in CFB with bypass ducts. Process Safety and Environmental Protection, v. 91, n. 5, p. 386–390, 2013. Disponível em: <http://dx.doi.org/10.1016/j.psep.2012.08.004>.

USEPA, United States Environmental Agency. Air Pollution Control Cost Manual: Particulate Matter Controls. EPA/452/B-02-001. . [S.l.]: North Carolina, NC. , 2002

VERSTEEG, H. K.; MALALASEKERA, W. An Introduction to Computational Fluid Dynamics: The Finite Volume Method. [S.l: s.n.], 2007. v. 2.

WANG, L. K.; PEREIRA, N. C.; HUNG, Y.-T. Air pollution control engineering. [S.l.]: Springer,2004. v. 1.

WORLD HEALTH ORGANIZATION (WHO). **Health effects of particulate matter:** Policy implications for countries in eastern Europe, Caucasus and central Asia. WHO, 2013.

ZHANG, Jinping; LI, Angui. CFD simulation of particle deposition in a horizontal turbulent duct flow. Chemical Engineering Research and Design, v. 86, n. 1 A, p. 95–106, 2008.

APPENDIX A

The initial mesh was made with refinements in regions that demand more attention, such as deflectors, small curves, and walls that promote high gradients, known as inflation, which capture the effects of the boundary layer.

Two lines were drawn in the region downstream of the deflectors at the beginning of the straight segment that decomposes to the exits to the fabric filter chambers. In these lines, the velocity profiles were analyzed (Figure 23) to compare the different meshes.

Figure 23: Location of the lines drawn for the mesh test.

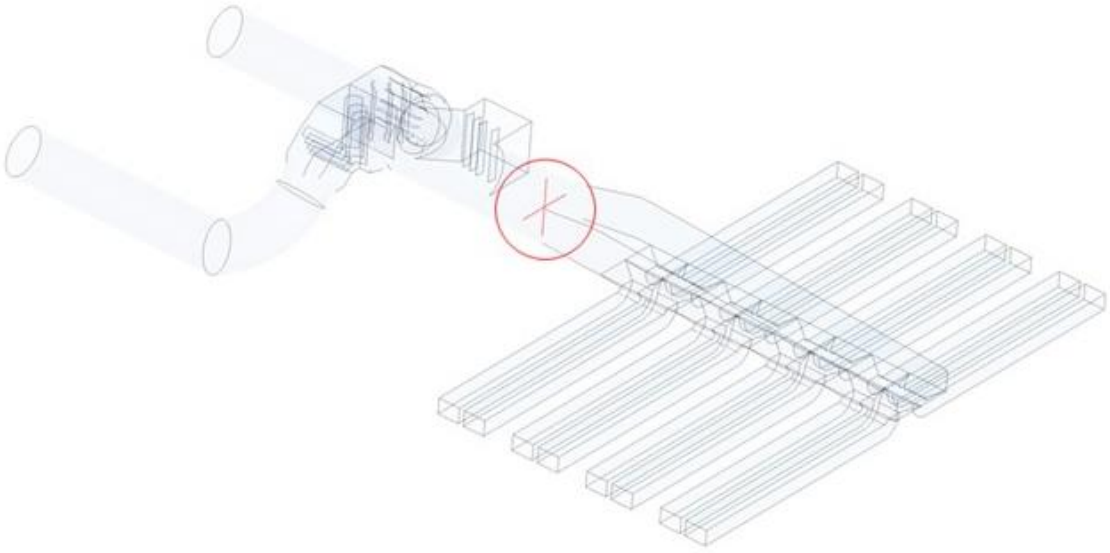

The dimensionless y + parameter of the wall was also observed. According to Verteeg and Malalasekera (2007), for values $30 < y^+ < 500$, the modeling in the vicinity of the wall is satisfactory. If the value does not fit this range, further refinement on the wall is necessary. This parameter indicates whether the number of elements in the boundary layer is adequate to represent its effects. It is worth noting that the highest values of y^+ found were in the deflector region, which is why the more considerable attention is given to them.

Thus, the parameters, as mentioned earlier, were evaluated for different meshes, indicated in Table 9.

Table 9: Characteristics of the meshes used for the test.

Mesh	Nº elements	Observation
1	6,1 mi	Realizable $k-\varepsilon$ turbulence model
2	7 mi	A bigger number of layers in the inflation and same turbulence
3	9,5 mi	A smaller element size in the deflectors and same turbulence model
4	11,2 mi	A bigger number of layers in the inflation and smaller element size in the deflectors with SST $k-\omega$ turbulence model

The evaluation of velocities v and w in the vertical and horizontal lines, respectively, indicated little variation in the different meshes, as shown in Figure 24 and 25.

Figure 24: Comparison between the velocities found on the vertical line for the four meshes.

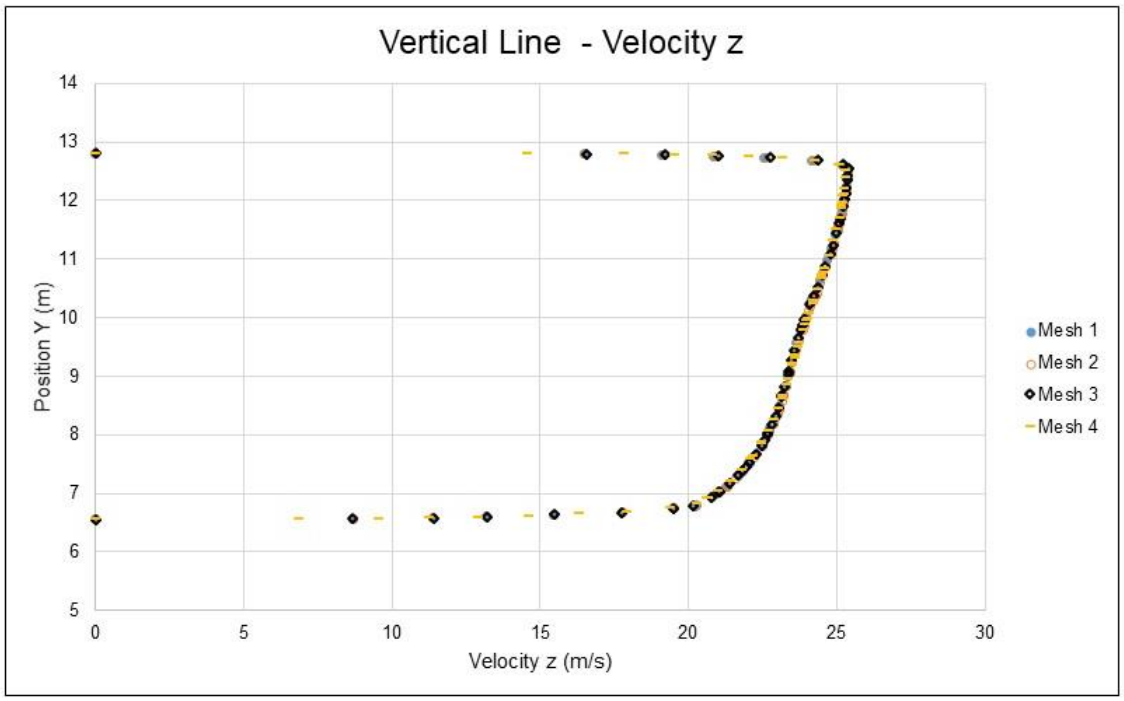

Figure 25: Comparison between the velocities found on the horizontal lines for the four meshes.

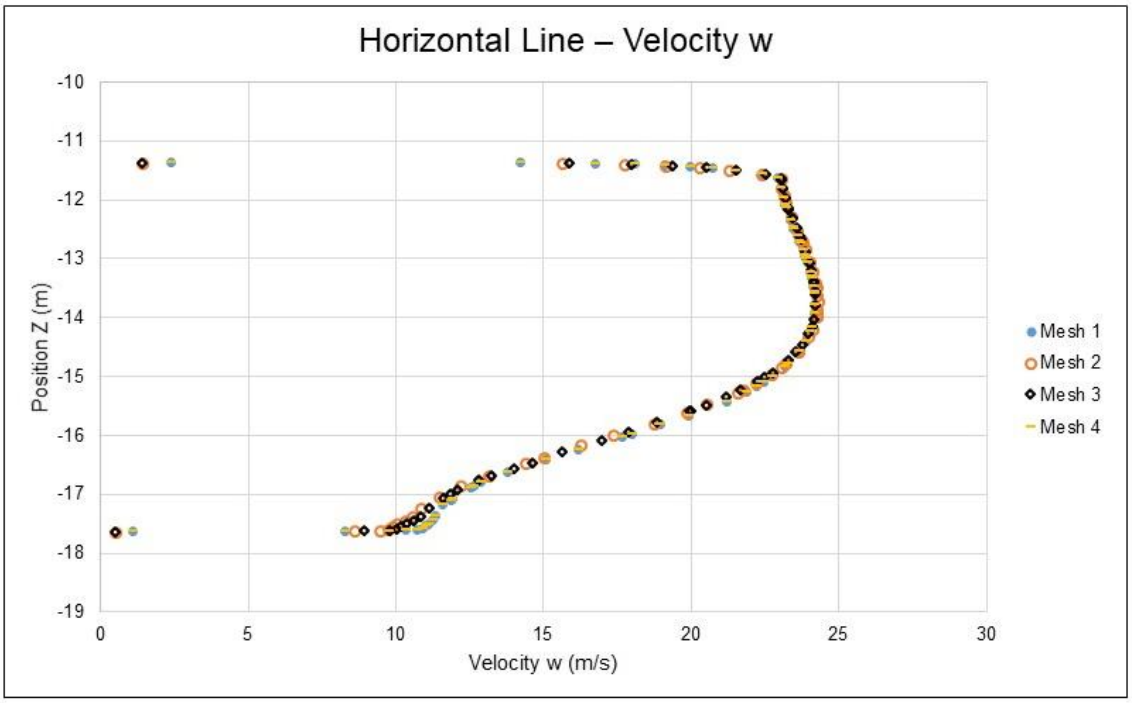

Analyzing the similar velocity profiles in the vertical and horizontal lines, the determining factor for choosing the mesh was the value of y+ and the demand for computational resources. In none of the cases was the y+ interval extrapolated, except for mesh 4, in which the SST $k-\omega$ turbulence model was used.

In mesh 4 with 11,2 million elements, for simulations using the SST $k-\omega$ turbulence model, Verteeg and Malalasekera (2007) indicate that the model has better accuracy in the region close to the walls, compared to the Realizable $k-\varepsilon$ model, being necessary, for this, y^+ equal to 1. It was observed that y^+ max equal to 300, so to reach the value of $y^+=1$, it would be necessary to increase the refinement in inflation, requiring high computational effort or even making the simulation unfeasible. Therefore, the mesh 1 of 6,1 million elements with the Realizable $k-\varepsilon$ turbulence model was the most optimized.